The Upper Critical Field of Niobium-Titanium

by

HENRY JOHN MULLER

A thesis submitted in partial fulfillment of the
requirements for the degree of

Doctor of Philosophy
(Materials Science)

at the

UNIVERSITY OF WISCONSIN-MADISON
1989

Contents

1 Introduction

The WHH theory[1] is one of the most widely used theories of H_{c_2}, the upper critical field at which superconducting behavior is suppressed. Originally proposed in 1966, this theory was first tested against data on Nb-Ti measured by Neuringer and Shapira[2], which it appeared to fit quite accurately. However, when it was used to describe the behavior of other systems, the agreement was not as good. Hawksworth and Larbalestier[3] noticed that tantalum additions to the Nb-Ti system raised the H_{c_2} value to such an extent that the WHH theory no longer agreed with experiment. At about the same time, Orlando et. al.[4] suggested a modification to the basic theory which would reduce the disagreement between predicted and measured H_{c_2} for the Nb_3Sn and V_3Si systems. This correction, based on the renormalization treatment of the electron-phonon interaction, had been suggested earlier by Clogston[5], but was not fully developed.

This revision of the WHH theory seems physically well founded, but the behavior of Nb-Ti has not been examined in light of this revision. The earlier studies of Nb-Ti[2][3] concluded that the material was paramagnetically limited, with H_{c_2} reduced below the depairing limit by the paramagnetic moment of the normal state material. Renormalization corrections alter this picture and greatly reduce the importance of paramagnetic limitation effects. In this study, a set of Nb-Ti alloys, fabricated and metallurgically characterized previously by Moffat[6], was examined. The revised WHH parameters for each of these alloys were derived from electromagnetic and thermal measurements, and the predicted H_{c_2} values based on these values were compared to the measurements.

The first section is a general overview of the metallurgy of the Nb-Ti system. The second, third, and fourth sections present metallurgical, chemical, and structural information about the eight alloys used in this study. This information has been previously published in greater detail by Moffat and Larbalestier[7]. Sections five, six and seven present resistivity, critical field, and critical temperature data for these alloys, as well as experimental details concerning the measurement of these quantities. Section eight describes the heat capacity measurement apparatus, and section nine briefly compares the calorimetrically measured critical temperatures with those measured using other techniques. In section ten, the heat capacity data is presented and analyzed using the Debye model to determine the electronic heat capacity coefficient. Section eleven compares this electronic heat capacity to that predicted by the GLAG theory, one of the precursors of the WHH theory. Section twelve outlines the WHH theory, while section thirteen examines the revisions to this theory suggested by Orlando et al.[4], and experimental schemes for determining the parameters of this theory. The harmonic lattice approximation for the lattice specific heat is reviewed in section fourteen, and a method for extracting phonon density of states from heat capacity data is presented. In section fifteen, critical field data is compared to the predictions of the revised WHH theory, and discrepancies are discussed.

2 The Nb-Ti System

The Nb-Ti system exhibits two stable phases, hexagonal close packed α-titanium and body centered cubic β-niobium.[8] There are also some metastable phases which are created when the alloy is cooled rapidly from relatively high temperature: there are two martensitic variants of α, and the ω phase, which are hexagonal derivatives of the BCC lattice.[9] It is possible to freeze in the β phase structure and suppress formation of other phases with a sufficiently rapid quench from a temperature at which only β phase exists (above about 700°C). The quench rate necessary to prevent transformation depends strongly on composition and is very large for the titanium rich alloys (about 3000 K/s for Ti18at.%Nb).[10]

According to a model proposed by DeFontaine[11], the ω phase can also exist in a virtual state, a temporary structural excitation of the BCC lattice, if the $2/3 < 111 >$ phonon mode has sufficiently low energy. Neutron diffraction measurements show that even pure niobium exhibits pronounced softening of that mode.[12] Vohra has maintained, based on band structure calculations and measurements on ω phase alloys, that the stability of the β lattice against this transformation to ω should decrease as the d-electron concentration is reduced.[13] In Nb-Ti alloys, this occurs as titanium concentration increases. Thus, even if the metallurgical phase of a sample is pure β, some signs of this virtual ω can be expected, such as diffuse x-ray scattering into areas of the reciprocal lattice associated with the ω structure. Such scattering has been studied by Balcerzak and Sass[14], and by Moffat and Larbalestier.[7]

3 Preparation of Alloy Samples

The Nb-Ti alloys in this study were prepared by Moffat[6] for a comprehensive study of the phase relationships of the system. They were used in this study because they were fully characterized microstructurally and are believed to be as close to single phase, homogeneous alloys as it is possible to obtain. What follows is only a brief review of the sample preparation, since full details have already been published.[6][7]

These samples were melted in a titanium gettered argon atmosphere from commercial purity niobium (99.9 atomic percent) and titanium (99.7 atomic percent) rods. These rods were chemically etched before arc melting, using a mixture of HF and HNO_3. The ingots were inverted and remelted at least ten times, and weight loss during this process corresponded to less than 1/2 atomic percent in every case. The ingots were then homogenized in niobium foil lined silica tubes. Because these tubes begin to soften at the homogenization temperature of 1300°C, they were filled at room temperature with 20 kPa of gettered argon, to prevent collapse at high temperature. The samples were quenched by breaking the silica capsules containing them under water. The homogenized ingots were swaged from irregular cylinders with about 8 mm mean diameter to 3 mm diameter rods, an true strain of 2.

Chemical impurity analysis was conducted at this point, and the samples showed noticable hydrogen contamination (about 1/2 atomic percent), due to the water quench, so they were subjected to a vacuum anneal in 10^{-3} Pa argon at 800°C for 3 hours. After this anneal, the hydrogen impurity levels decreased by about an order of magnitude, while the other impurities remained within a factor of 2 of their levels before annealing. Cold work from swaging was reduced by a recrystallization treatment at 1000°C. Since the capsules were rigid at that temperature, this anneal was conducted in a gettered argon atmosphere of less than 1 Pa. Since the diffusion constants for high niobium alloys are much lower than those for low niobium concentration, the heat treatment times were longer for the high niobium alloys.[6] The details of the heat treatment sequence and the results of impurity analyses are given in table 1. Each sample was finally quenched from the 1000°C anneal, as they had been from the 1300°C treatment, so it is likely that hydrogen contamination in the final samples is near the same level as it was after the first water quench. The interstitial content of these alloys are typical of those found in commercially produced Nb-Ti superconductor alloy.

Transmission electron microscopy and x-ray diffraction showed that the 20%

Alloy(at.%Nb)	20	25	30	35	40	50	60	70
Hrs at 1300°C	8	8	8	8	8	24	24	24

IMPURITIES AFTER QUENCH values in appm/wppm

C	-	-	$\frac{507}{100}$	-	-	-	$\frac{496}{80}$	-
N	-	-	$\frac{783}{180}$	-	-	-	$\frac{271}{51}$	-
O	-	-	$\frac{2133}{560}$	-	-	-	$\frac{1630}{350}$	-
H	-	-	$\frac{4535}{75}$	-	-	-	$\frac{3326}{45}$	-

IMPURITIES AFTER VACUUM ANNEAL appm/wppm

C	$\frac{755}{160}$	$\frac{785}{160}$	$\frac{865}{170}$	$\frac{739}{140}$	$\frac{656}{120}$	$\frac{526}{90}$	$\frac{746}{120}$	$\frac{791}{120}$
N	$\frac{445}{110}$	$\frac{193}{46}$	$\frac{257}{59}$	$\frac{181}{40}$	$\frac{211}{45}$	$\frac{186}{37}$	$\frac{203}{38}$	$\frac{249}{44}$
O	$\frac{2903}{820}$	$\frac{3019}{820}$	$\frac{3821}{1000}$	$\frac{2774}{700}$	$\frac{1930}{470}$	$\frac{1580}{360}$	$\frac{1634}{350}$	$\frac{2425}{490}$
H	$\frac{1068}{19}$	$\frac{993}{17}$	$\frac{546}{9}$	$\frac{692}{11}$	$\frac{456}{7}$	$\frac{418}{6}$	$\frac{\leq 371}{<5}$	$\frac{\leq 393}{<5}$

Hrs at 1000°C	8	8	8	8	24	24	24	24

Table 1: Heat Treatment and Impurity Analysis

niobium sample has an orthorhombic lattice, corresponding to the α'' martensite structure. The 25% sample also showed α'' martensite near the surface of the rod, but the core was BCC β phase. Careful examination of this core revealed very fine precipitates of ω phase. The remaining samples were all β phase throughout, but the diffraction patterns of the 30% and 35% alloys showed streaks in the reciprocal lattice image charecteristic of virtual ω. The intensity of these streaks was too low and diffuse to form an image of precipitates, so it is unlikely that ω is actually present. Additional optical microscopy, electron probe microanalysis, and back scattered electron imaging showed no compositional inhomogeneity in the samples. These techniques, in combination, have been shown to reveal 1 atomic percent variation in composition over a distance of about 1 μm.[15]

4 Resistivity Measurement

In the resistivity measurement apparatus shown in figure 1, a sample rod is held by two spring loaded copper rods, which serve as current contacts and also press the sample against knife edge voltage contacts. This four point measurement is uncertain to about 0.8%, principally due to variations in the diameter of the alloy rod. The measurement was conducted using a measuring current density of 0.1 A/mm^2 through the sample. Measurements at temperatures below 77K were performed in cold helium gas, and the temperature was adjusted by raising or lowering the sample in the stratified column of gas. The resistivity at T_c was measured at a height just above that at which resistance dissappeared in the sample.

As shown in figure 2, resistivity depends strongly on titanium concentration and only weakly on temperature. For all the single phase samples, the resistivity increases steadily with titanium content, and the temperature dependence, as measured by $\rho(300)/\rho(T_c)$, becomes weaker. In the 20% and 25% alloys, which are two phase materials, the resistivity ratio increases as titanium content increases. This agrees with earlier work on V-Ti[16] and Nb-Ti[17] which suggests that the soft phonon mode which exists in the BCC phase becomes more pronounced as composition becomes more titanium rich. The low energy phonons scatter electrons and increase resistance, but their population depends only weakly on temperature, at least at temperatures above T_c. Thus, as alloy composition nears the phase stability boundary, the resistivity ratio decreases. Once martensite formation occurs, the soft mode is suppressed, causing the resistivity ratio to increase again.

The resistivities measured in this study are compared in figure 3 to previously published data. In the 20% and 25% alloys, the data are widely scattered, which is not suprising in view of the wide variety of microstructures which are possible for different impurity levels and sample heat treatments. The Berlincourt and Hake data are uniformly higher than other data, though with the same composition dependence. This may be due to the cold work present in their samples, which can enhance resistivity[19], or perhaps due to the generally higher interstitial con-

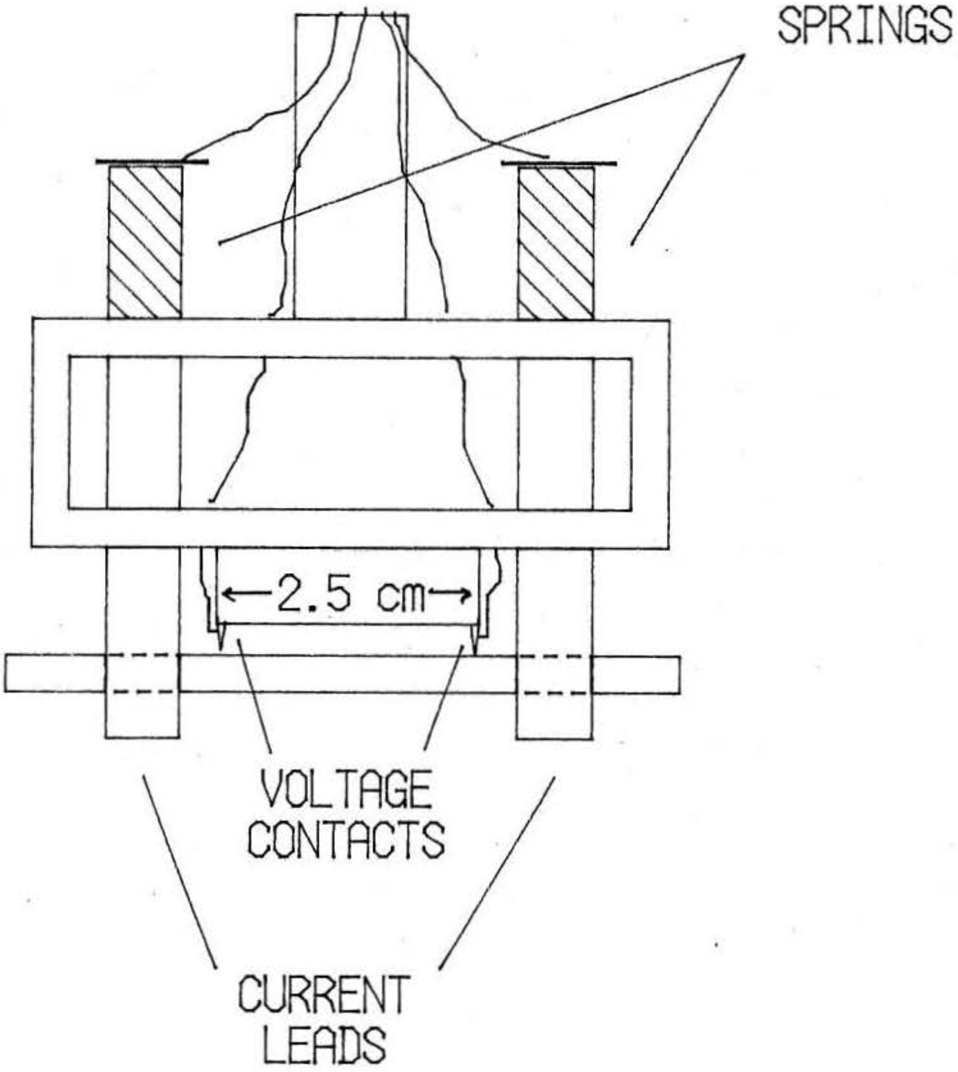

Figure 1: Resistivity Measurement Apparatus

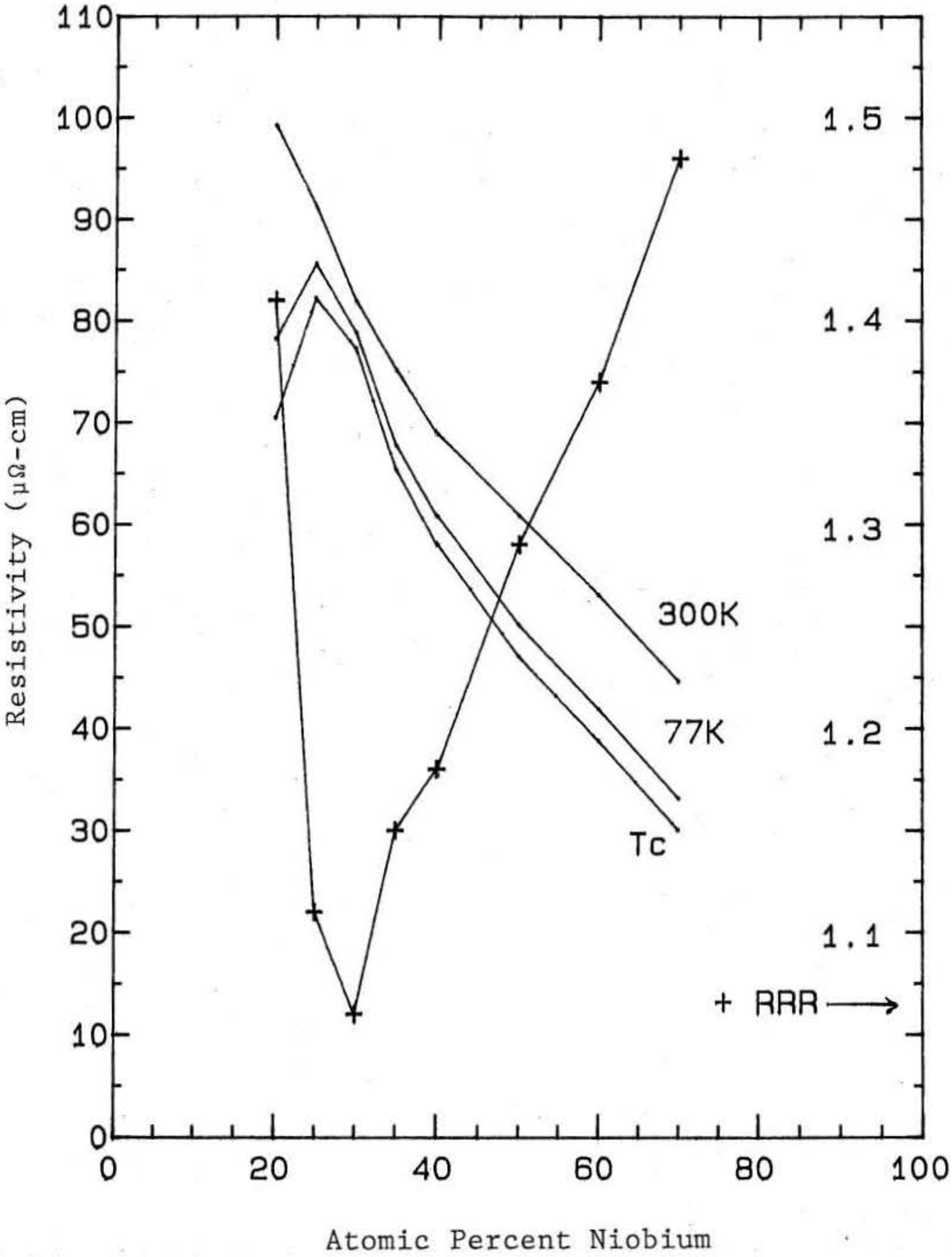

Figure 2: Resistivity and RRR as a Function of Composition

tent of these early alloys. The results of the present study seem reasonable for recrystallized samples.

5 Upper Critical Field Measurements

The H_{c_2} measurement apparatus is similar to that used for making resistivity measurements, with current and voltage contacts pressed against a sample rod. Here, however, the separation between voltage contacts is about 8 mm. Also, two thermometers are mounted on the copper current lead rods in contact with the sample. One of these thermometers is a capacitance sensor, used to control sample temperature in the presence of a magnetic field. The other thermometer, a germanium resistor, is used to calibrate the capacitance sensor, since this sensor changes calibration each time it is heated or cooled past 60K, at which point a phase transformation occurs in the sensor material [20]. For measurements above 4.2K, the entire apparatus is placed inside a can containing low pressure helium gas, and the gas temperature is controlled using an ohmically heated shroud. At temperatures below 4.2K, the apparatus is immersed directly in liquid helium, and the temperature is adjusted by changing the pressure of gas above the bath, thereby changing the boiling temperature of the liquid.

Previous investigators [3][21] have noted that measuring current density can affect resistively based H_{c_2} measurements. For the samples in this study, less than

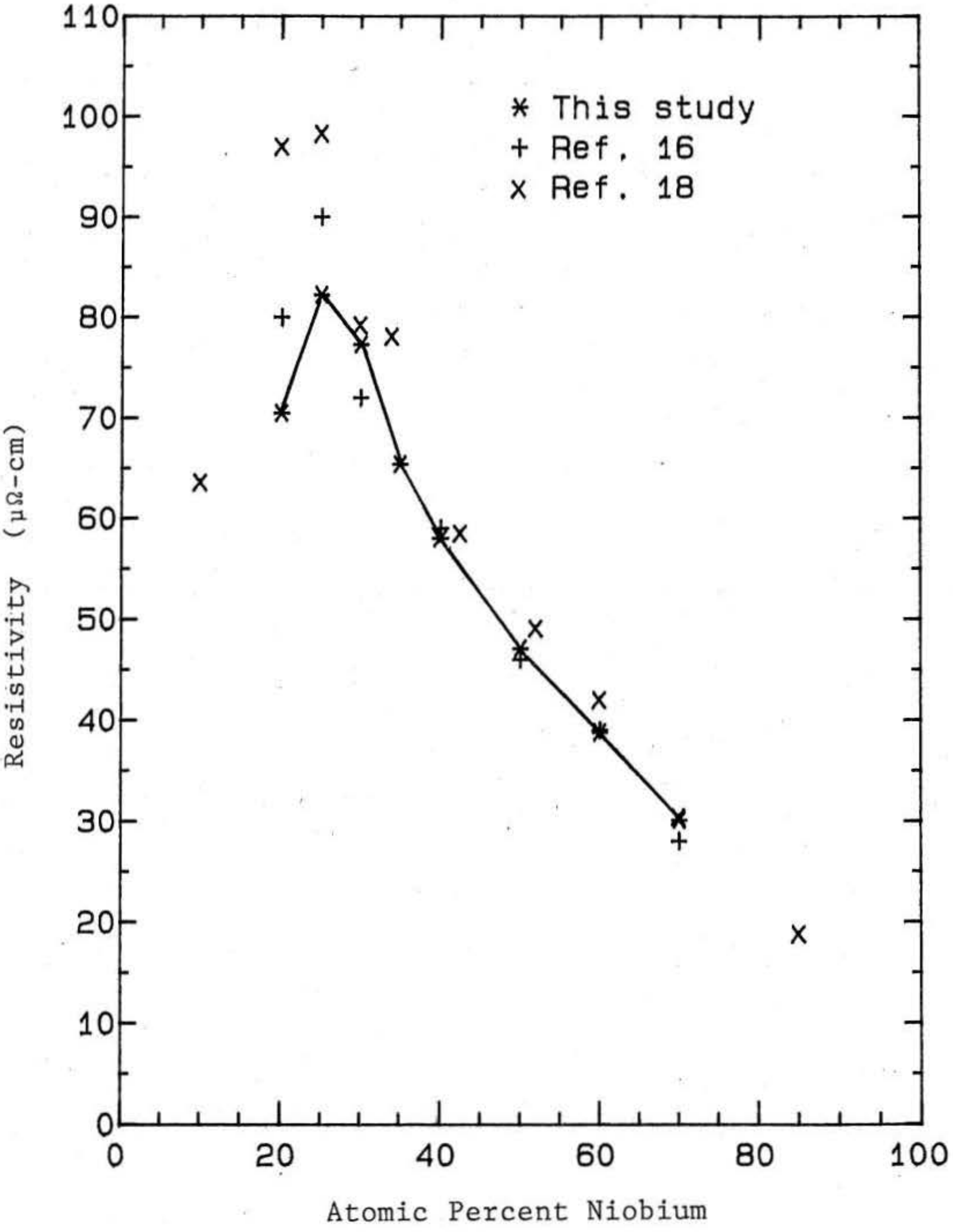

Figure 3: Comparison of Resistivity Data

0.02 Tesla variation in H_{c_2} was found with measuring current densities ranging from 0.1 mA/mm^2 to 10 mA/mm^2. The shape of the transition was similarly unaffected, and for nearly all the samples the transition width (temperature spacing between points at which 10% and 90% of normal state resistivity was achieved) was about 0.1T. A measuring current density of 1 mA/mm^2 was used for all the data in this section, and $H_{c_2}$was taken to be the point at which resistivity equaled one half that of the normal state.

All data for temperatures 4.2K and above were collected at the University of Wisconsin using a 13T superconducting magnet system. The data at 4.2K and below were collected using one of the Bitter solenoid magnets operated by the Francis Bitter National Magnet Laboratory at MIT. The H_{c_2}(4.2K) data at both locations agreed within 0.3T. These data are presented in figures 4 through 11.

The H_{c_2} values at 4.2K are compared in figure 12 to those published in previous studies. The maximum value measured in this study was 11.6T, for the 35% Nb alloy. There is general agreement about the shape of the H_{c_2}versus composition plot between the various data sets, but the actual spread in values can exceed 2 T. The data of Bellin et. al. are unusually high for compositions between 50% and 80% Nb. This study used a different criterion for H_{c_2} than the others, marking it at the field at which $J_c(B)$ drops "rapidly", rather than the field at which resistivity rises to some sizable fraction of that of the normal state. However, this criterion should reduce rather than raise the critical field. At present, these results are unexplained. Another discrepancy occurs for the 25% and 30% Nb alloys of the present study, which have higher H_{c_2} values than those in other studies. Data presented in the next section shows that the T_c of these alloys are also unusually high, so it is likely that the H_{c_2} elevation is a consequence of structural differences resulting from their controlled thermal treatment.

According to the WHH theory, the value of dH_{c_2}/dT near T_c (above about $.8T_c$) should depend linearly on temperature[1]. This limiting slope is indeed constant for all the alloys studied, and it is indicated on the H_{c_2} plots (figures 4-11). The errors associated with this limiting slope are based on the coefficient uncertainty of a linear least squares fit to the high temperature H_{c_2} data. The trend in dH_{c_2}/dT is the same as that in H_{c_2}itself; the peak of both curves is near the 30% composition, though the contrast between maximum and minimum values is much smaller for the critical field slope than for the upper critical field. The maximum value of the slope is 3.25 T/K, exhibited by the 30% Nb alloy, while the minimum value, found in the 70% Nb alloy, was 1.5 T/K.

6 Transition Temperature Measurement

There are several ways to define the critical temperature of a superconductor. Traditionally, electrical resistivity is monitored while the sample is heated until the zero resistivity state disappears. Since a supercurrent can be sustained as long

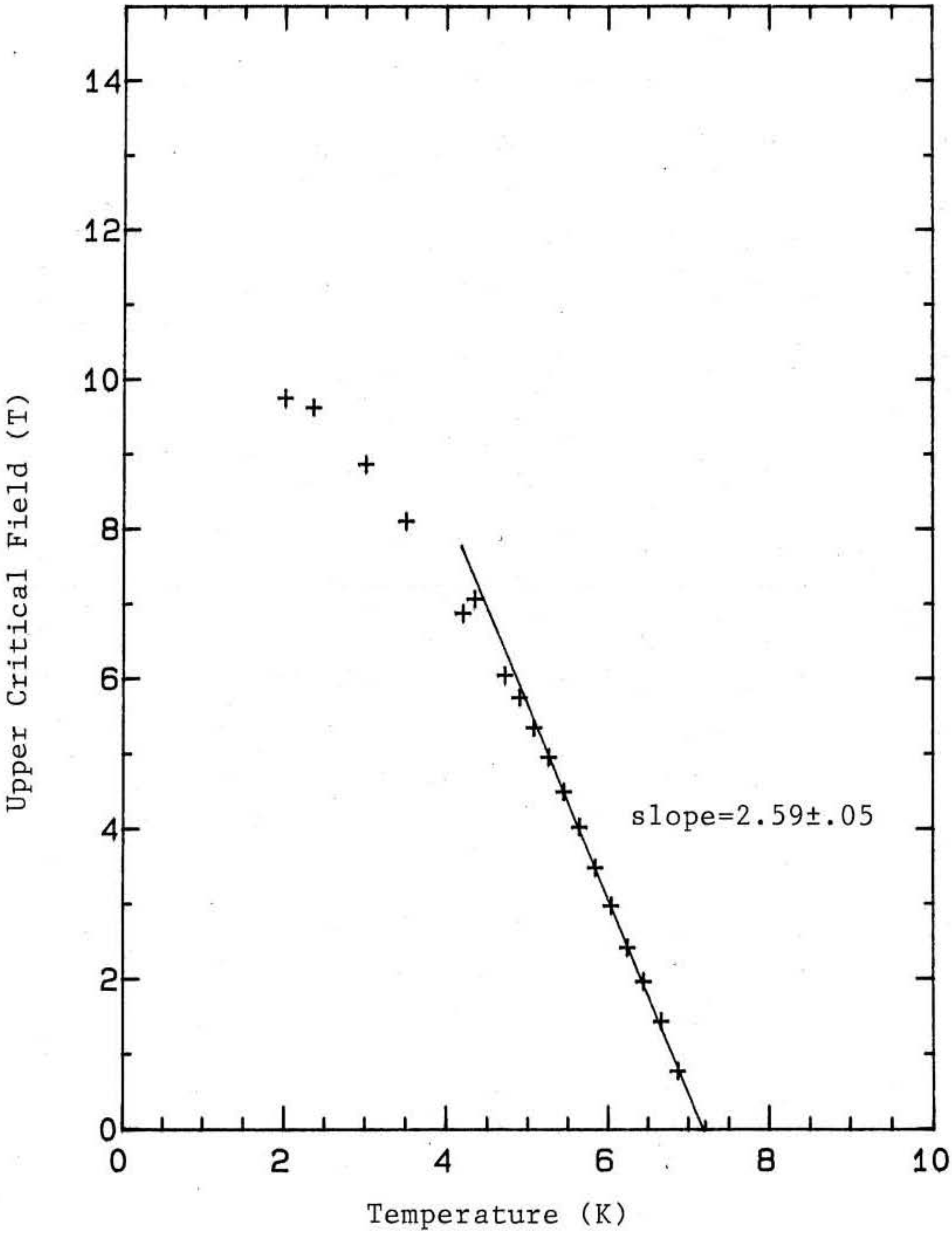

Figure 4: H_{c_2} versus Temperature for 20% Nb Alloy

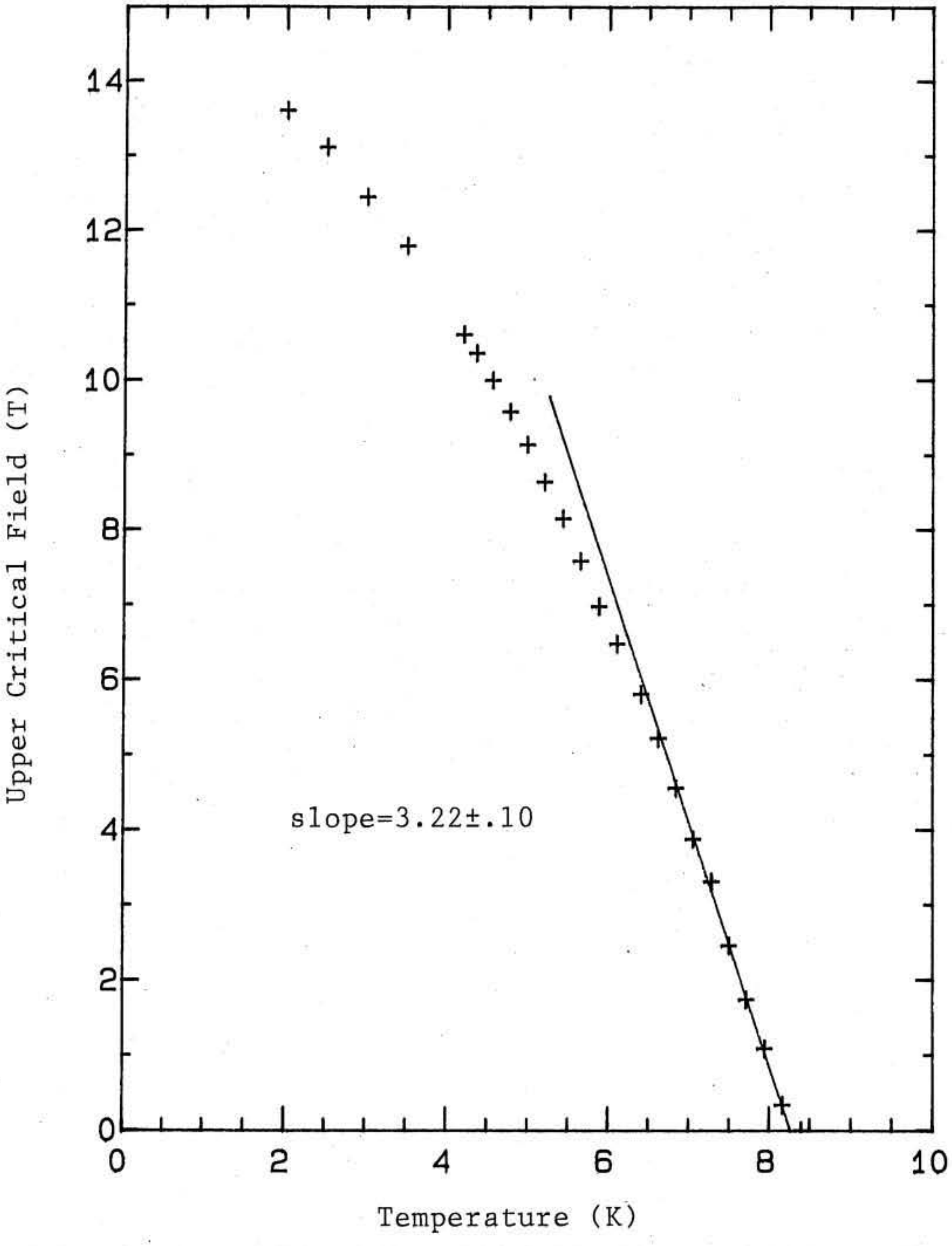

Figure 5: H_{c_2} versus Temperature for 25% Nb Alloy

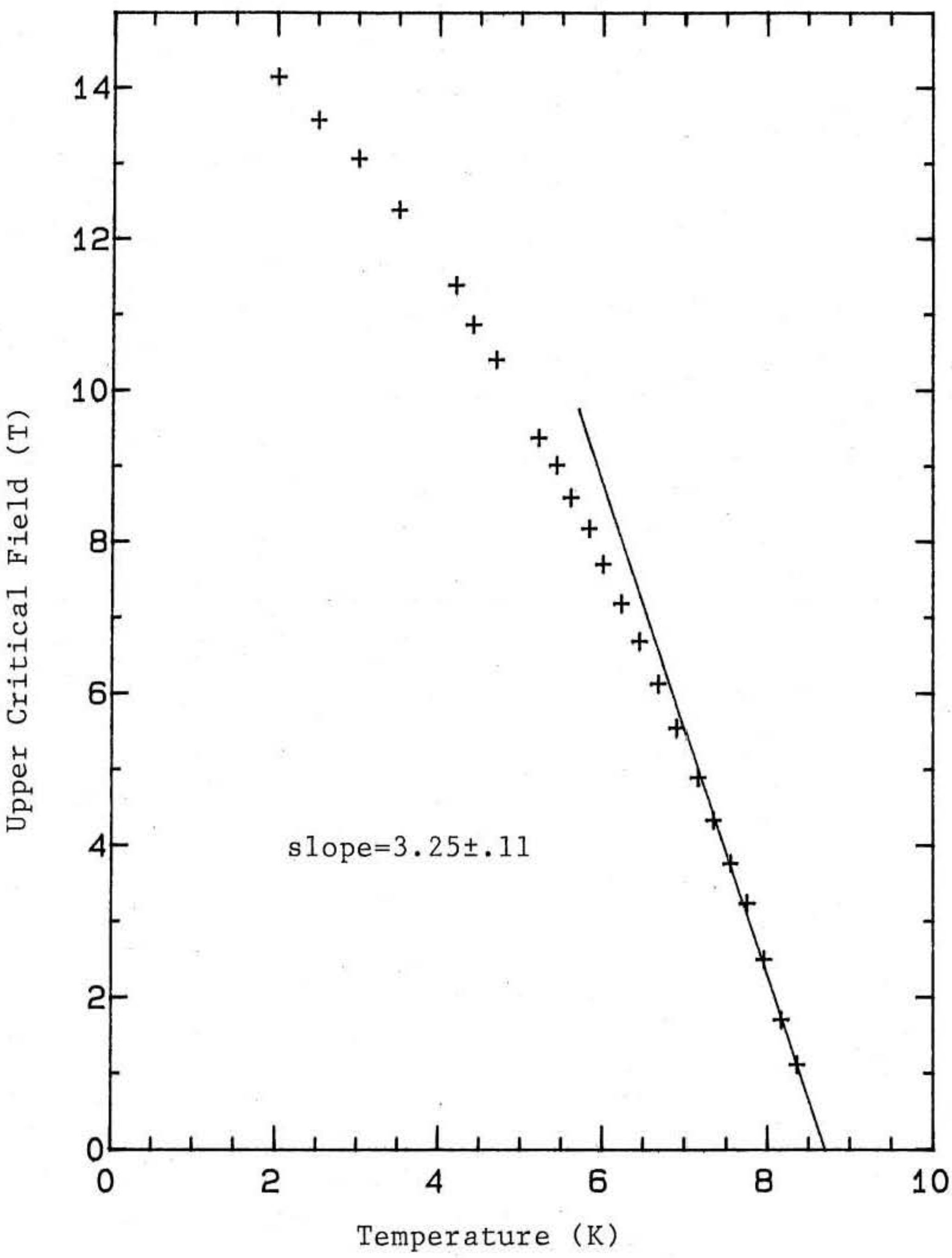

Figure 6: H_{c_2} versus Temperature for 30% Nb Alloy

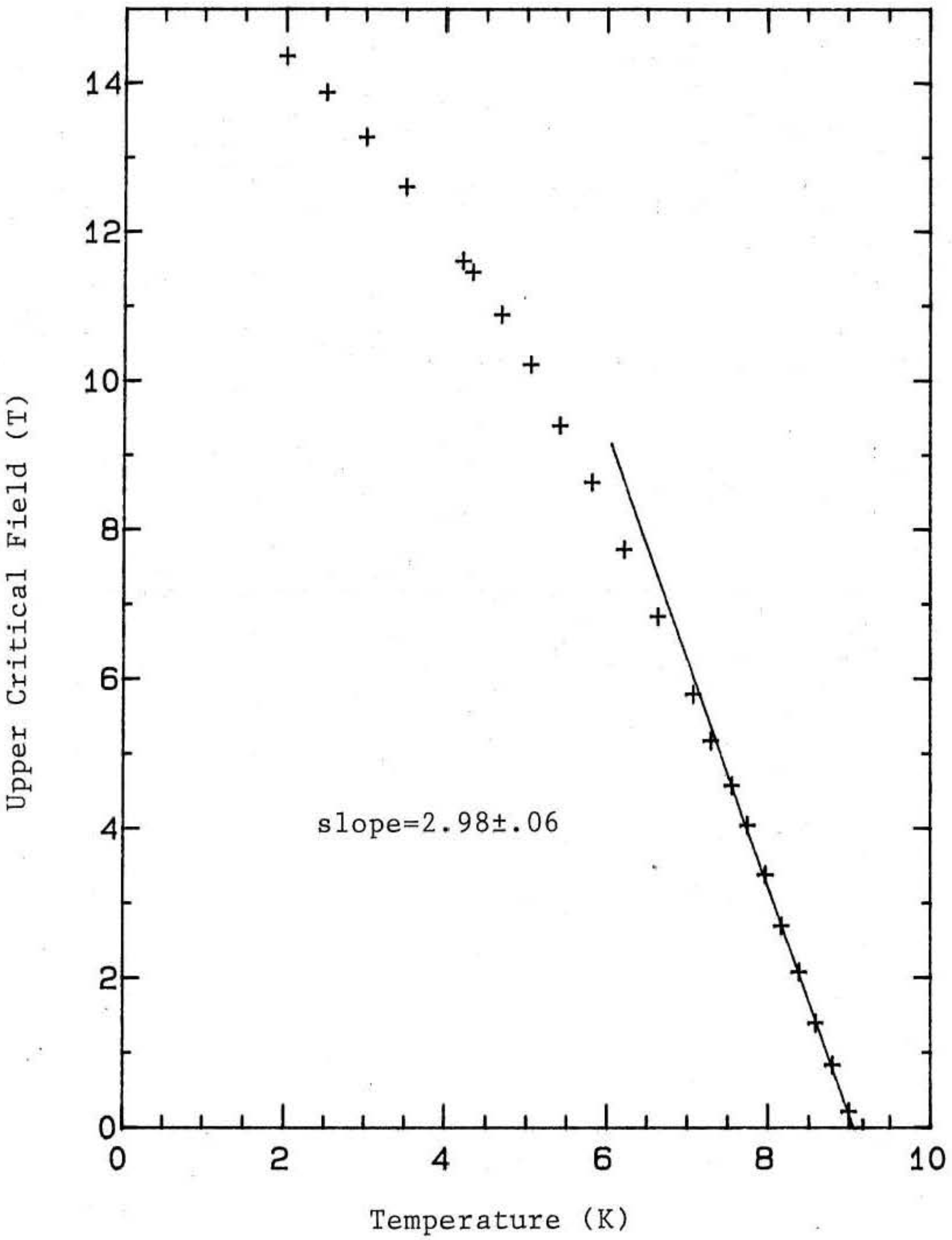

Figure 7: H_{c_2} versus Temperature for 35% Nb Alloy

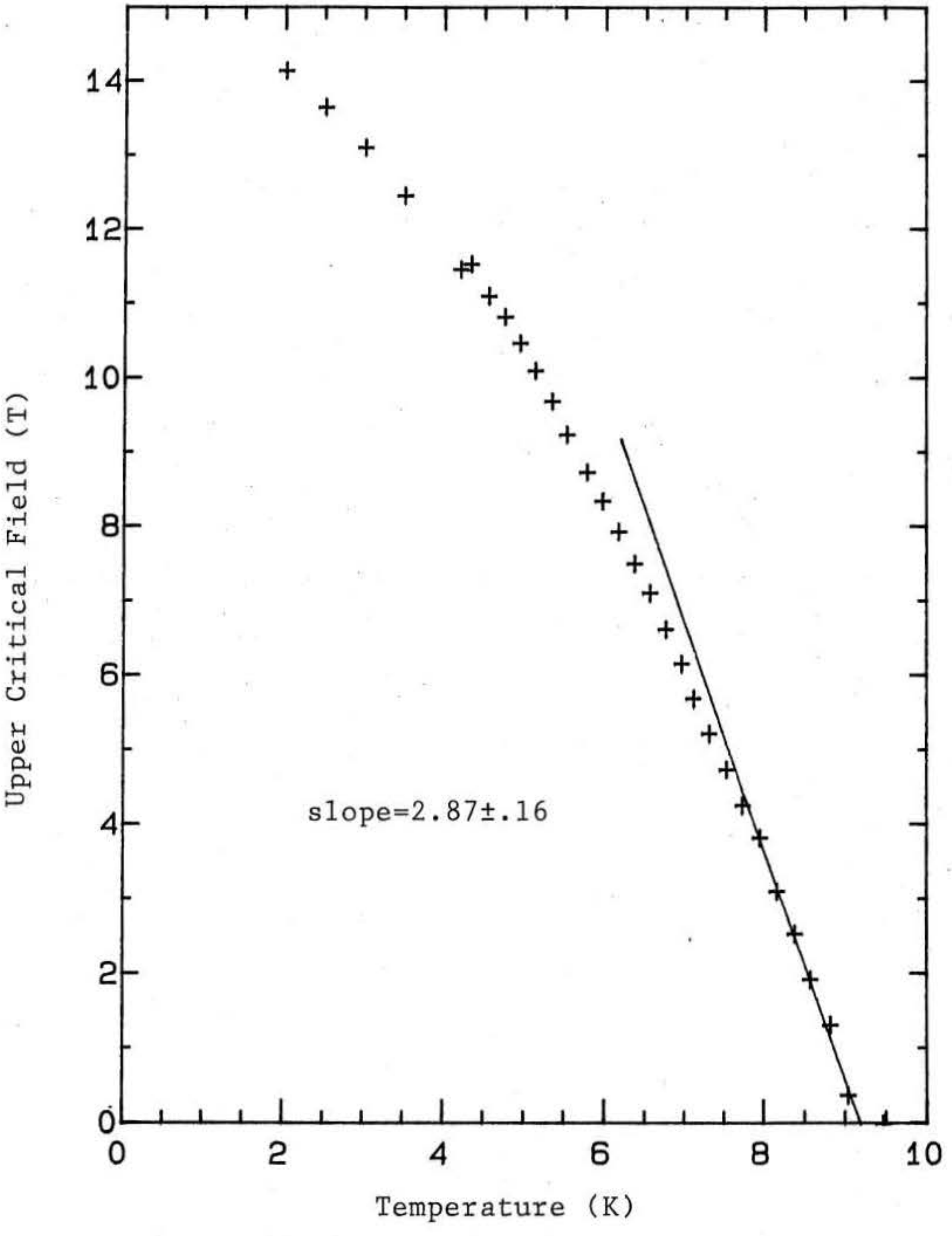

Figure 8: H_{c_2} versus Temperature for 40% Nb Alloy

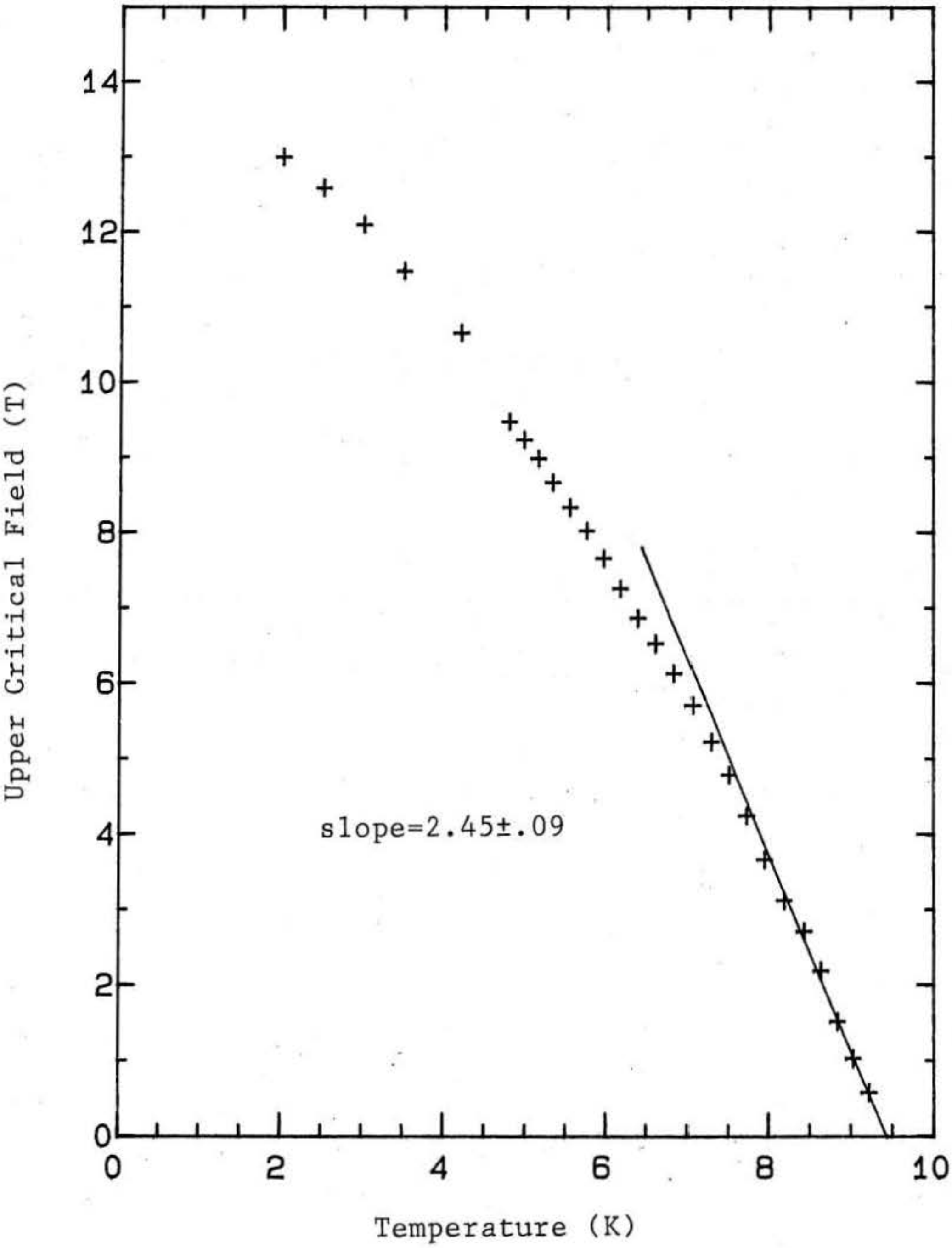

Figure 9: H_{c_2} versus Temperature for 50% Nb Alloy

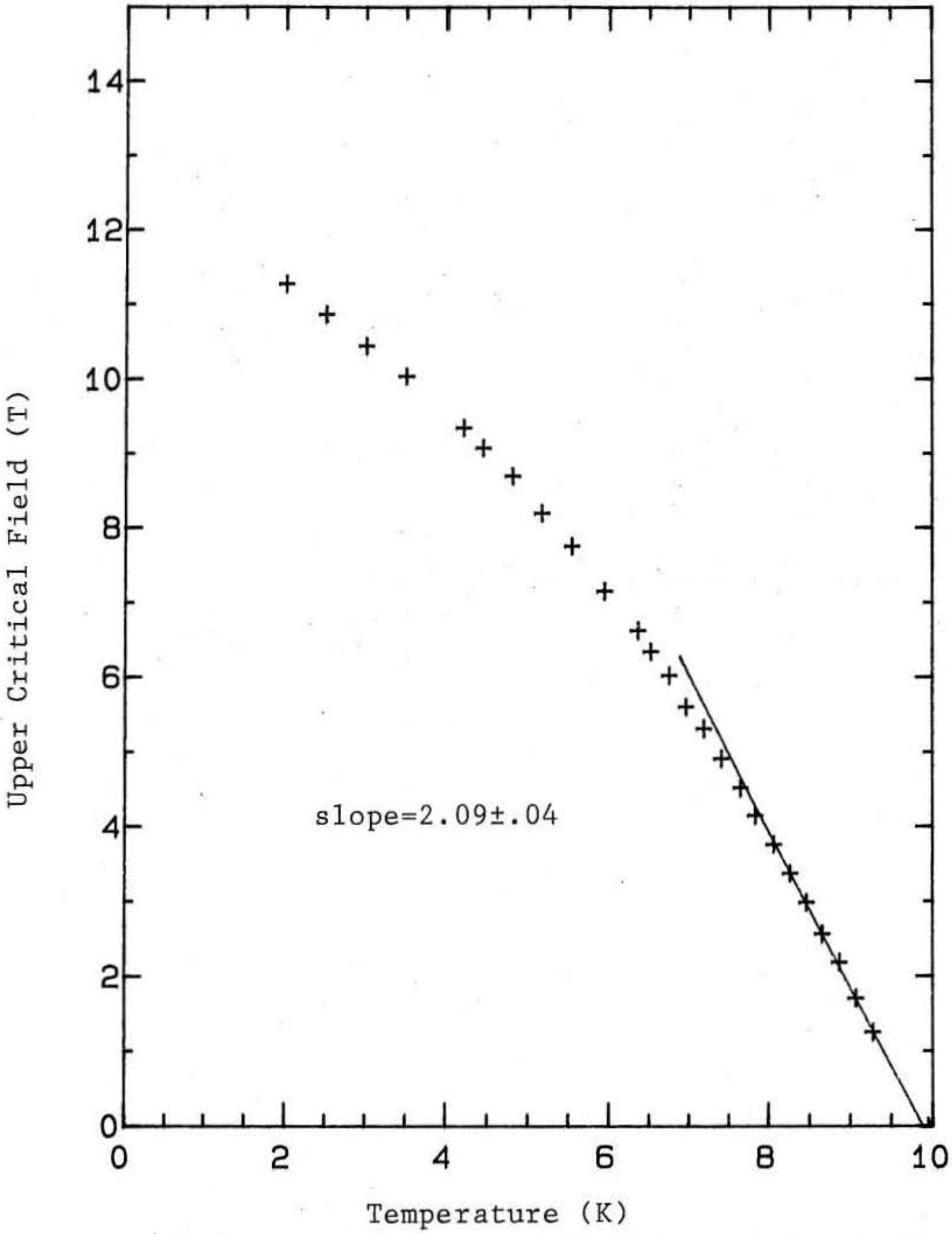

Figure 10: H_{c_2} versus Temperature for 60% Nb Alloy

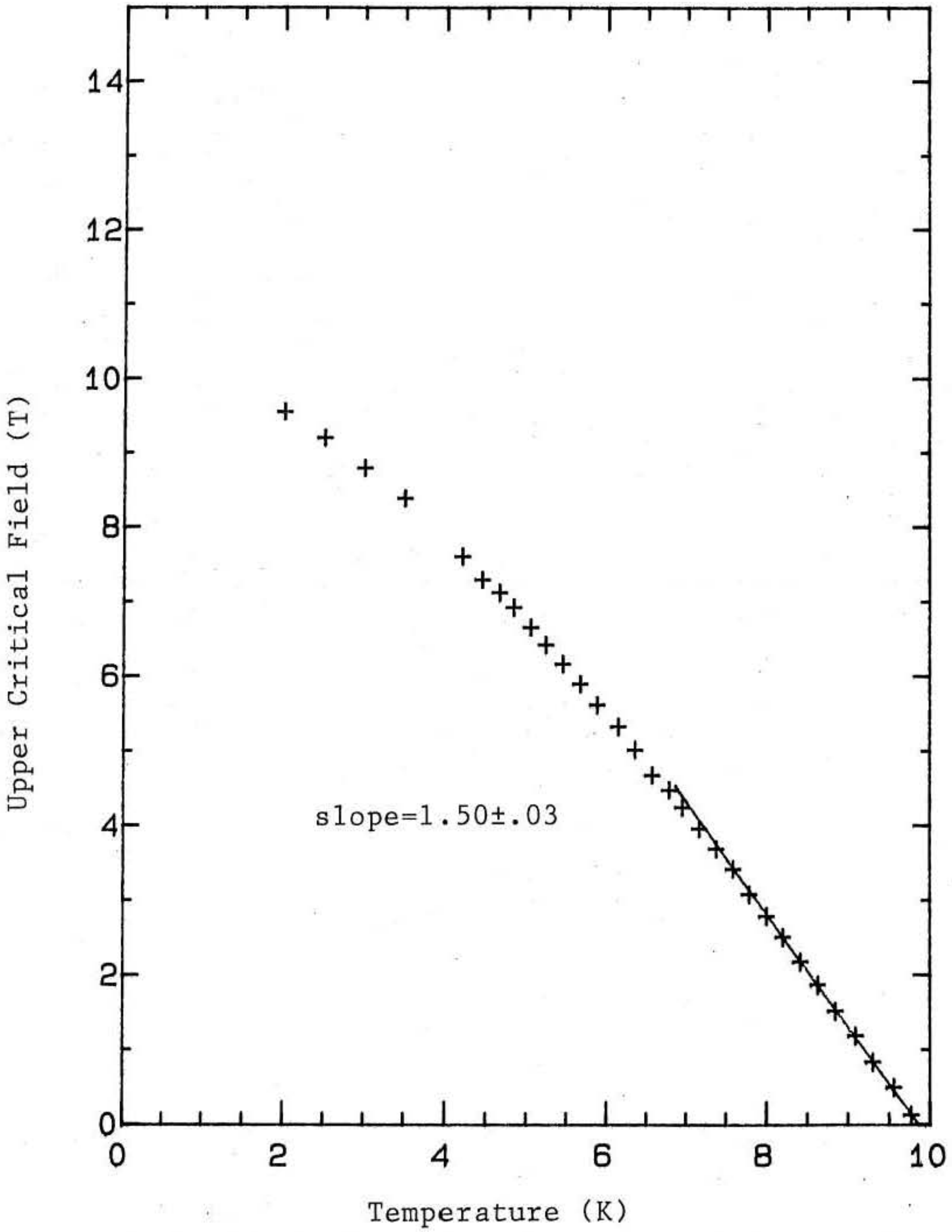

Figure 11: H_{c_2} versus Temperature for 70% Nb Alloy

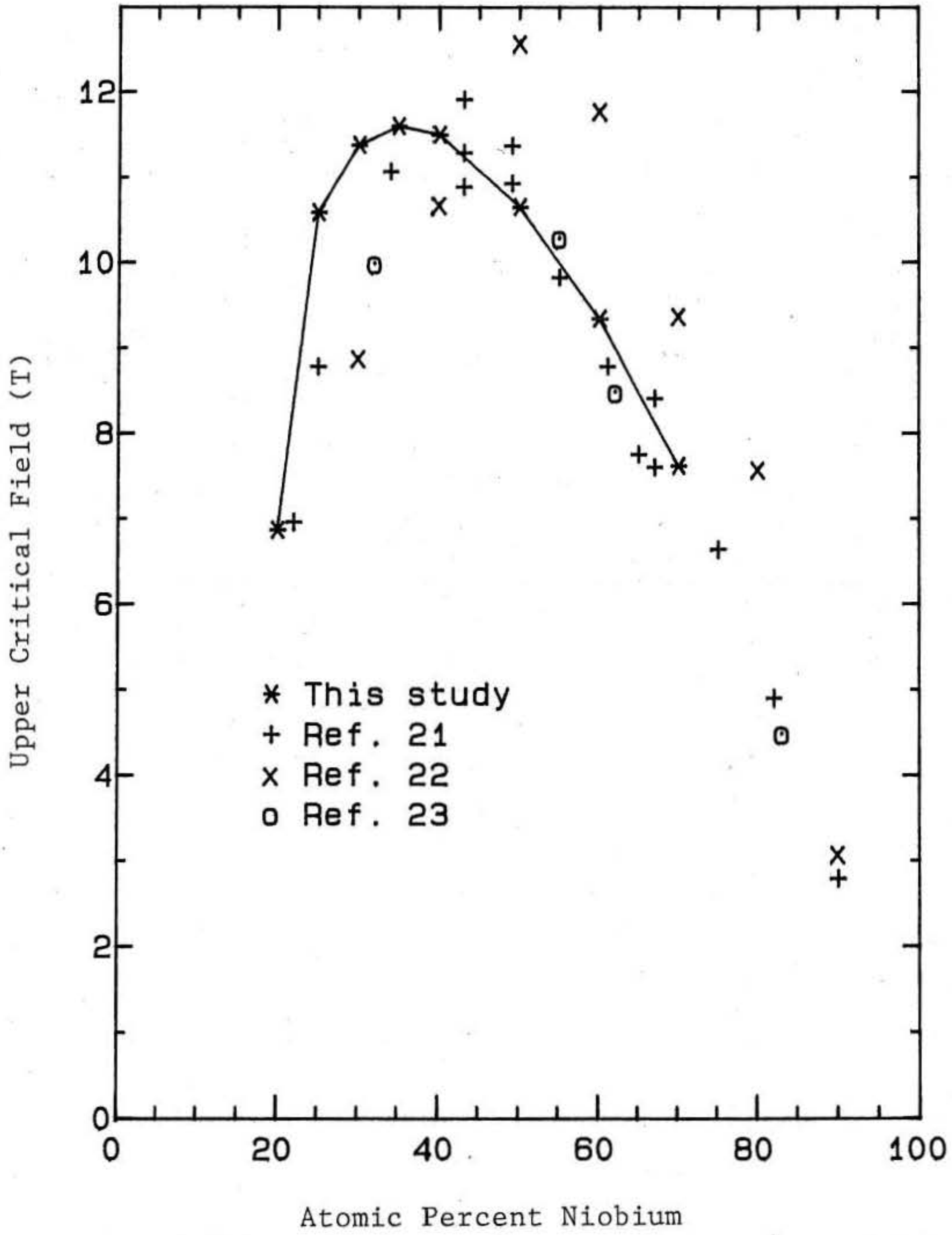

Figure 12: Comparison of H_{c_2} Results

as a filamentary superconducting path exists, the resistive transition is usually quite sharp, and can occur when most of the sample is already normal. In this study, the resistive T_c is taken to be the midpoint of the resistive transition, while the width is the spacing between the 10% and 90% values.

Another measure of T_c comes from extrapolating H_{c_2} versus T data to the intercept at $H_{c_2}=0$. This critical temperature is the most appropriate one to use in the WHH model, since it is based on the assumption of a linear H_{c_2} temperature dependence which results from the theory. The chief determinant of the uncertainty in this extrapolated T_c is the width of the H_{c_2} transition. Depending on what criterion is used for H_{c_2}, the zero field intercept can be moved over a range given by ΔH_{c_2}, the transition width, times the inverse limiting slope, dT/dH_{c_2}.

Yet another method involves measuring the susceptibility of the sample. At T_c, the superconducting sample undergoes a change from the diamagnetic Meissner state ($\chi = -1$) to the paramagnetic normal state ($\chi \approx 10^{-5}$). The apparatus used in this study is a dual coil AC bridge susceptometer with a variable temperature sample holder[24]. This experiment operates at 17 Hz and has a sensitivity limit 1000 times smaller than the signal caused by the sample transition at T_c. The inductive technique examines surface screening currents, so it is not always sensitive to microscopic inhomogeneities. However, if there is gross segregation in a sample, so that the surface properties are different from those at the core, an unrepresentative T_c can result. In the case of the 25% alloy, the inductive measurement shows two distinct transitions, one at 7.6K, and another smaller one at 8.1K, as shown in figure 13. The lower temperature one probably corresponds to flux exclusion from the α'' phase outer layer, while the higher transition is due to flux exclusion from the β phase core. The inductive signal should be proportional to the volume of the sample which is excluding flux, so the relative transition magnitudes imply that about 20% of the sample is β phase. None of the other samples shows a double transition.

Figure 14 presents a comparison of inductively measured T_c results from a number of studies. T_c rises to a maximun of 9.88K at 70 at. % Nb, the same composition at which Suenaga and Ralls found a maximum T_c of 10K. In general, the present data shows T_c changing smoothly with composition, in contrast to the scatter of earlier data. The scatter of this earlier data seems greater than can be accounted for by simple thermometer calibration differences. Certainly there can be questions about whether the structural state of the samples near Ti25at.%Nb are all the same, and this could account for the wide spread of results near that composition. This explanation should not hold for the niobium rich alloys, but these are precisely the alloys most difficult to homogenize. An additional issue is the generic and substantial problem of oxygen or other interstitial contamination, but this argument cannot be pursued fully for lack of sufficient chemical analyses. The smooth variation of T_c of the present alloys is believed to result from the care and uniformity of their preparation.

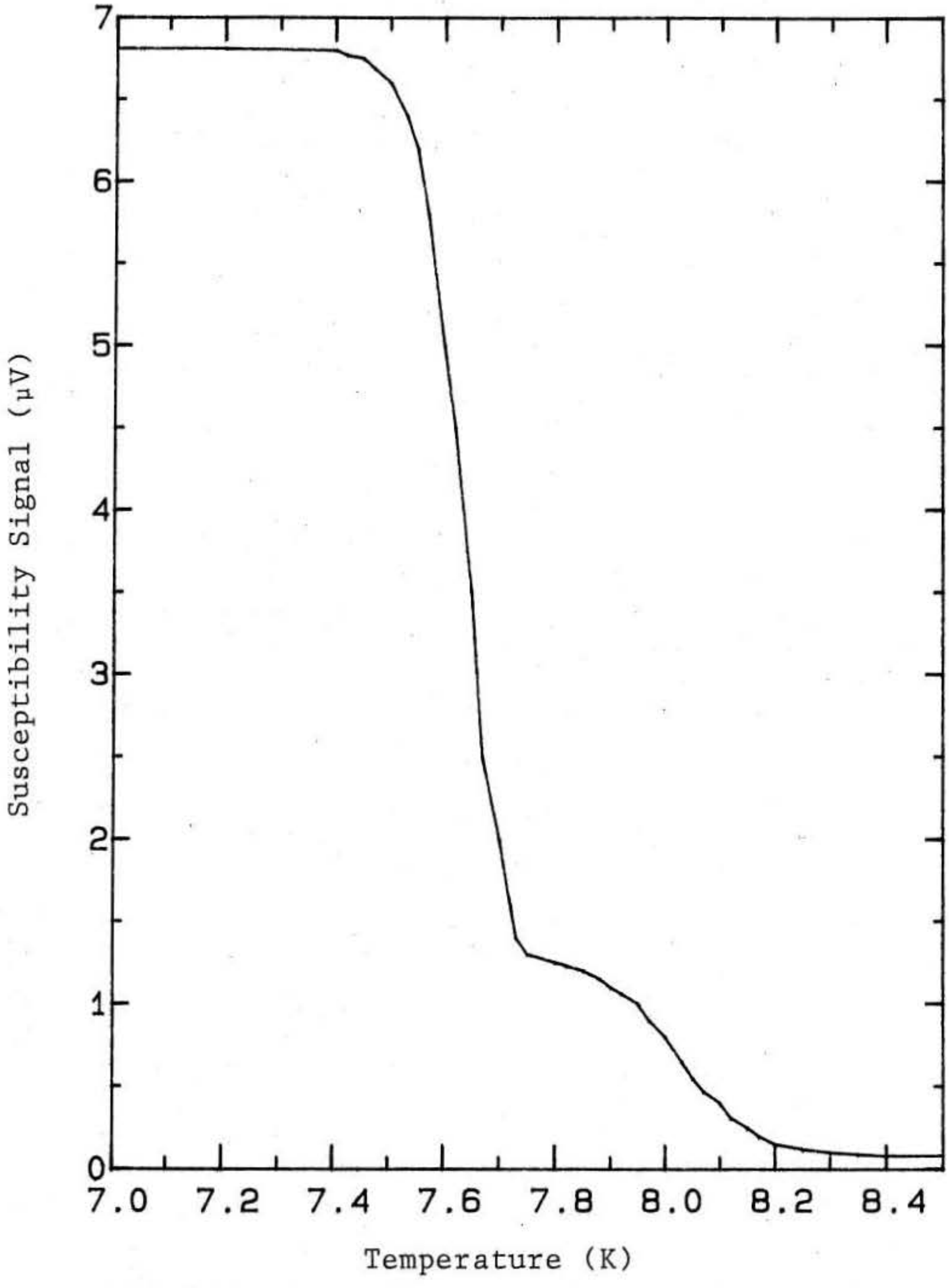

Figure 13: Inductive T_c Transition of 25% Niobium Alloy

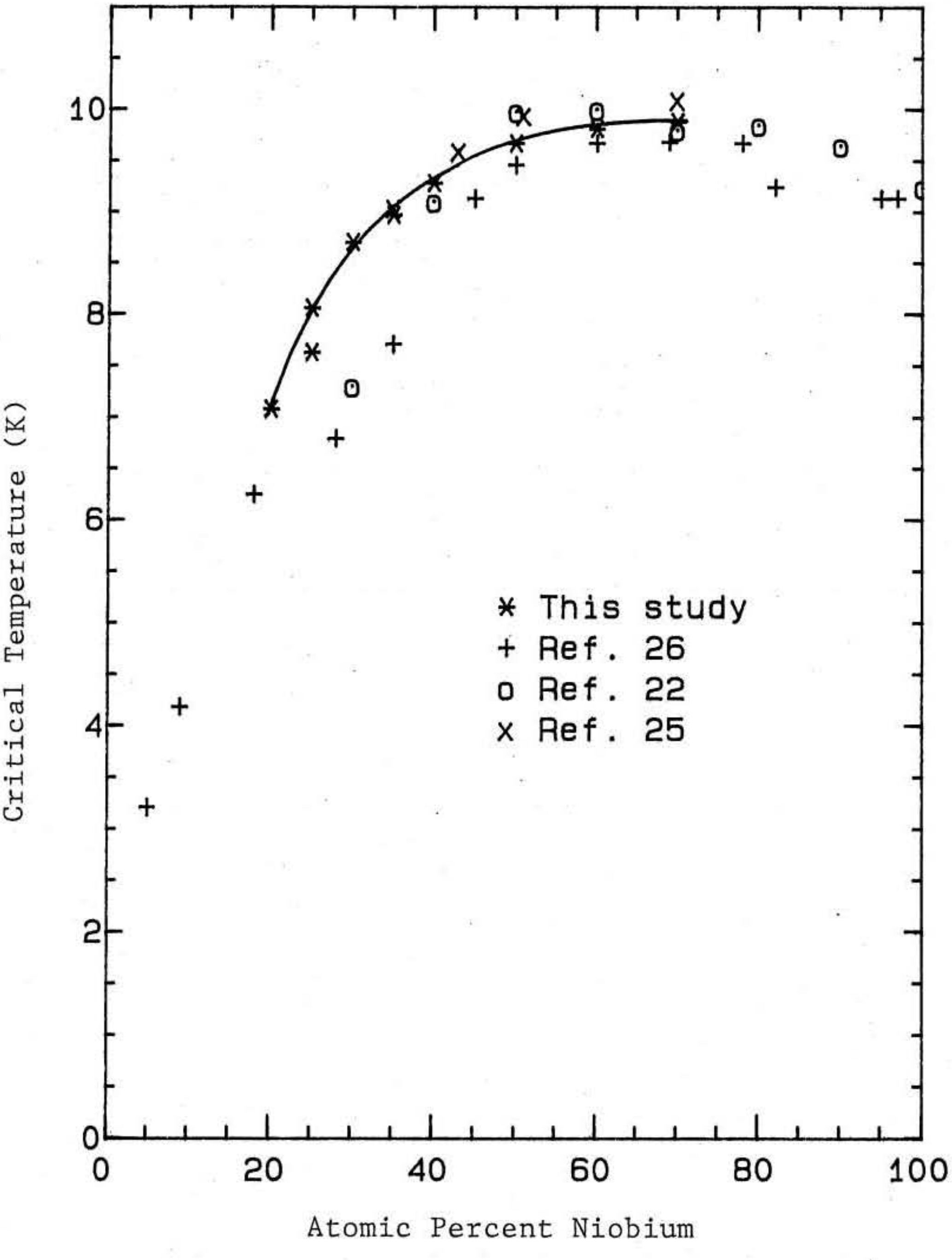

Figure 14: Comparison of Inductive T_c Data

7 Heat Capacity Measurement Apparatus

The apparatus used in the heat capacity experiment is shown in figure 15. It consists of a sample holder, with thermometer and heater, a thermal weak link, and a heat sink. The sample holder is a sapphire wafer 3 cm x 1 cm x .5 mm, to which is varnished a 350 ohm strain gauge heater and an unencapsulated germanium resistor. The thermal weak link, made up of several parallel coils of manganin wire (100 μm diameter) also serves as electrical connection to the heater and thermometer. The heat sink is a tube of high conductivity copper which is wetted on one end with helium at 4.2K. A sample rod is varnished in place with about 5 mg of GE 7031 varnish, and the entire apparatus is operated in a vacuum of less than 10^{-4} Pa pressure.

The calorimeter, similar in design to those of Forgan and Nedjat[27] and Lawless et al.[28], operates as a relaxation calorimeter. This technique requires that the sample and sample holder be in thermal equilibrium as they both slowly drift in temperature, in response to heat input or removal. If C_s is the sample heat capacity and C_a is the heat capacity of the experimental addenda, then simple thermodynamics yields the following:

$$(C_s + C_a) = dU/dT \tag{1}$$

Since dU/dT is the heat flux into or out of the addenda-sample combination, it

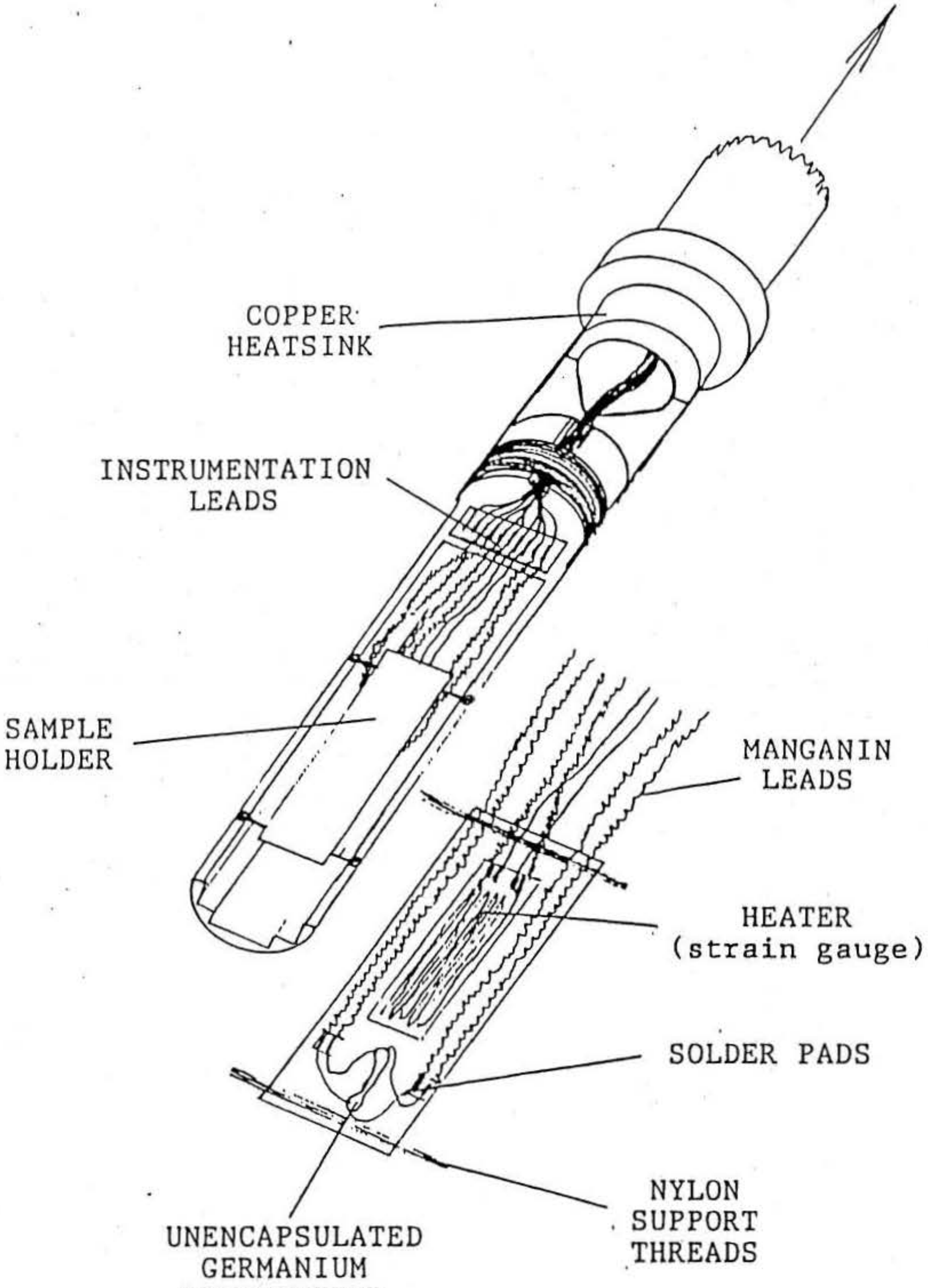

Figure 15: Heat Capacity Measurement Apparatus

can be expressed as the difference between P_i, the heat introduced by the heater, and P_o, the heat conducted away by the thermal link. The equation then becomes:

$$(C_s + C_a) = (P_i - P_o)dt/dT \tag{2}$$

From this, it is clear that the heat capacity can be calculated if the cooling rate and heat flow are both known.

The term in the equation above which is most difficult to evaluate is P_o. This is because it is the only one which can not be monitored during the experiment. It is possible to measure the equilibrium sample temperature for a variety of heater power settings, and thus obtain an accurate calibration of the heat leak, but the process is time consuming. Riegel and Weber[29] combine heating and cooling curves to eliminate the variable P_o, so that this lengthy calibration process can be avoided. The present study also uses this technique, but with different heater power conditions. In the Riegel and Weber study, the heater power was held constant during the heating cycle, and turned off during the cooling cycle, so that the drift rate, which was intially high, decreased dramatically near equilibrium. The accuracy of the measured drift rate deteriorates outside some optimum range, so many staggered measurement cycles were necessary to cover a large temperature range. In the present study, heater power was continuously adjusted so that the difference (P_i-P_o) was of constant magnitude throughout both heating and cooling cycles. In this way, dT/dt was kept near optimum over a wider range of temperature.

If P_o is the actual heatleak out of the sample and (P_o+P_e) is the calibrated heat leak, containing an error term P_e, then the operating equations for the calorimeter become the following:

$$C = \frac{(P_h - P_o)}{(dT/dt)_h} = \frac{(P_c - P_o)}{(dT/dt)_c} \tag{3}$$

Here, the subscript c denotes a cooling run, h denotes a heating run. Now, the experiments are conducted under constant drive conditions, that is:

$$P_h = P_o + P_e + K \tag{4}$$

$$P_c = P_o + P_e - K \tag{5}$$

K is referred to as the drive power. Under these constraints, equation 3 can be reexpressed as follows:

$$C(dT/dt)_h = P_e + K \tag{6}$$

$$C(dT/dt)_c = P_e - K \tag{7}$$

Now, combining both heating and cooling information:

$$C = \frac{2K}{(dT/dt)_h - (dT/dt)_c} \tag{8}$$

We can define heat capacities determined from either the heating or cooling curve alone, C_h and C_c:

$$C_h = \frac{K}{(dT/dt)_h} \tag{9}$$

$$C_c = \frac{K}{(dT/dt)_c} \tag{10}$$

These quantities are afflicted by systematic errors due to heat leak miscalibration, and are not equal to the actual heat capacity unless P_e=0. However, these quantities can be substituted into equation 8, for a further definition:

$$C = \frac{2C_hC_c}{(C_c + C_h)} \tag{11}$$

Using these formulae, it is possible to derive the heat capacity and correct for systematic errors due to heatleak miscalibration, using a set of heating and cooling data taken over the same temperature range. Since the experiment was run under constant drive conditions, it was assumed that the magnitude of the heating and cooling drive powers were the same. In general, the correction procedure will work even if that constraint is not satisfied.

Because this experiment took so long to run, it was computer operated. As shown in figure 16, an Apple II+ computer, equipped with analog inputs and outputs, monitored heated voltage, heater current, and thermometer voltage, while it controlled heater voltage. Every 1.5 seconds, the heater power was measured and compared with an approximate heatleak calibration, and the heater voltage was adjusted to maintain constant drive power. The sample temperature was measured every 30 or 60 seconds. Using the Savitsky-Golay technique[30], a nine point moving, weighted average of these data was formed, mathematically equivalent to the derivative at the center point of a third order polynomial fit to the original nine point data group. The smoothed and differentiated data set was used to find C_s+C_a as a function of temperature, and this information was saved on disk at the end of each cycle. From several runs with an empty calorimeter, the addenda heat capacity was determined to an accuracy of about 3%. In all the measurements in this study, the addenda correction constituted less than 20% of the sample heat capacity, and so it added less than .6% to the error in that measurement.

The experiment is based on the assumption that the heat leak depends only on temperature and that the sample and sample holder are in thermal equilibrium. The first of these assumptions was checked by applying a constant heater power and observing long term temperature shifts. Over a period of three days, heatleak variation was less than 0.1%, and over the duration of a typical measurement cycle (about 3 hours), there was no noticible change. The second assumption was checked each run, at the sample's transition temperature. In all cases, with a temperature drift rate of between 1 and 3 mK/s, the heating and cooling transitions occurred within 10 mK of each other. This lack of hysteresis indicates that the sample and sample holder are at essentially the same temperature. The absolute

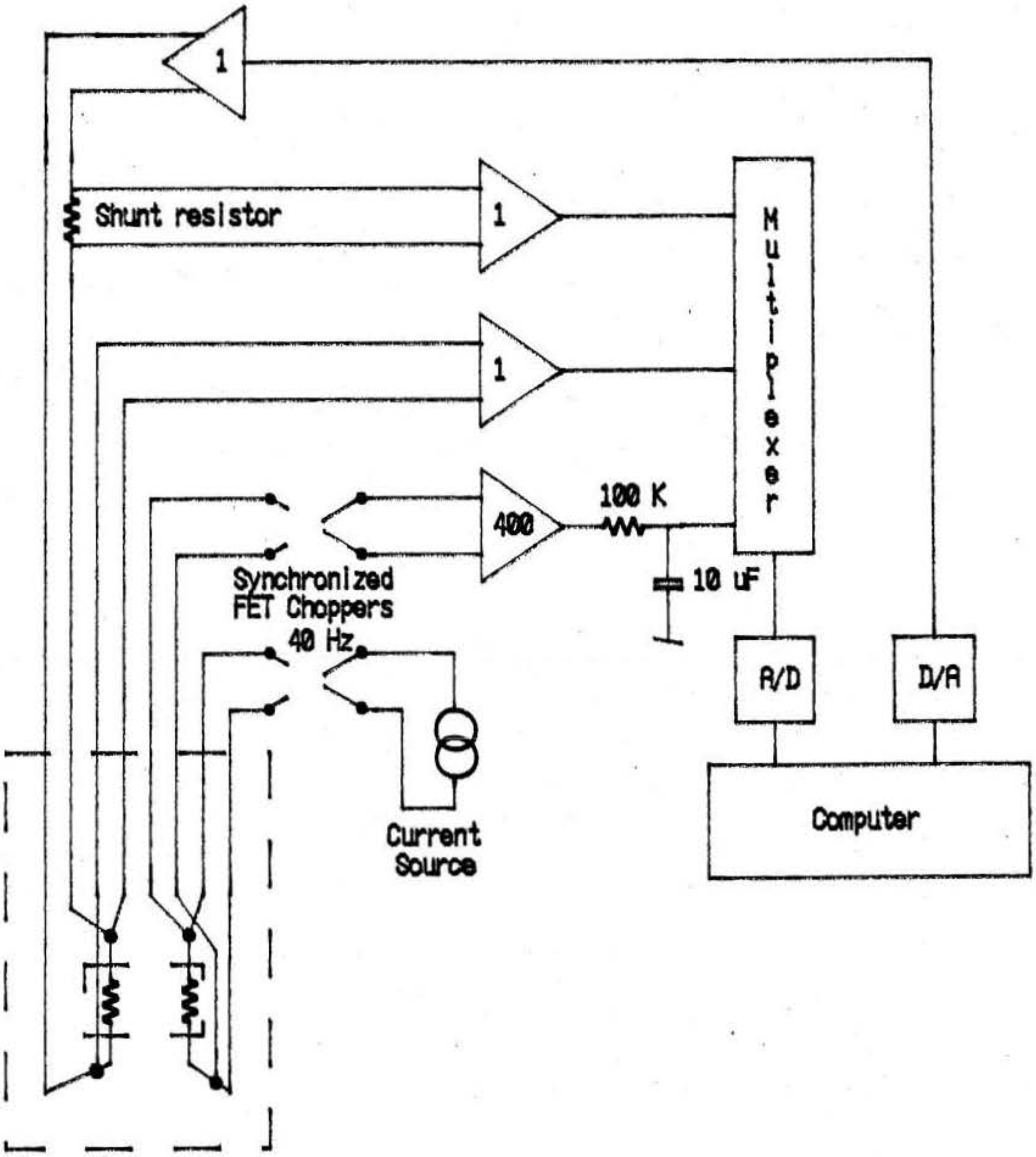

Figure 16: Heat Capacity Apparatus Schematic Diagram

temperature accuracy of this experiment was limited by long term drift in the thermometer electronics, on the order of 10 μV/month. This corresponds to a temperature drift at 10 K of about 30 mK/month. To correct for this effect, a high purity, homogenized niobium sample was run every few weeks, and the conductance bridge rezeroed to provide a constant transition temperature of 9.25 K. In all cases, these adjustments caused cumulative shifts of less than 50 mK. The standard sample, provided by Teledyne Wah Chang, had an inductive T_c of 9.25 K, a transition width of 70 mK, and a residual resistivity ratio of 250. A heat capacity measurement was performed on high purity copper (OFHC) at the beginning and end of this study. Both sets of data agreed with the copper reference polynomial of Osborne et al.[31] to within 3% from 6 K to 30 K. Spot checks against other data[32] at 35 K and 40 K were also within 3%.

8 Transition Temperature Comparison

The transition temperatures measured calorimetrically on the samples in this study are compared with the results of two other studies in figure 17. The error bars included illustrate the 10%/90% widths of each transition. These widths ranged from 0.22K to 0.39K, and seemed to be intrinsic, not an artifact of the smoothing which preceeds analysis. The widths are roughly the same as those found by Sasaki[33], which lends some support to the notion that this breadth is unavoidable even in good quality samples of Nb-Ti. The trend of the present data is smooth, with the exception of the Ti35at.%Nb alloy, which appears about 0.2K higher than the trend. By contrast, the data of Savitskii et al. is quite scattered. Sasaki's data is generally close to that of the present study, with an anomalously low point at Ti65at.%Nb.

As a final note in the comparison of critical temperatures, table 2 presents all the critical temperature information from the present study. The most clearly inhomogeneous material, the 25 at.%Nb alloy, exhibits a different T_c for each of the measurement techniques used. The resistive measure, which senses only the disappearance of the last filamentary superconducting path, gives the highest value (8.39K). The inductive measure, which signals the breakup of the sheath of screening currents on the sample surface, gives the next highest value (8.06K for the β phase region of the sample). The calorimetric measure, which records the average thermal response of each of the whole sample, gives the lowest value (7.72K). This behavior can be explained if there is a distribution of superconducting properties in the sample because it is microscopically heterogeneous. Microscopy and x-ray diffraction show that this is true for the 25 at.%Nb sample. It is interesting to note that a similarly broad T_c signature shows up in the 30 at.%Nb alloy, which shows no diffraction evidence of inhomogeneity. It seems likely that the incipient phase instability of this alloy, as evidenced by diffuse ω phase diffraction intensity, is contributing to the low T_c tail seen in the calorimetric T_c data. The spread in T_c

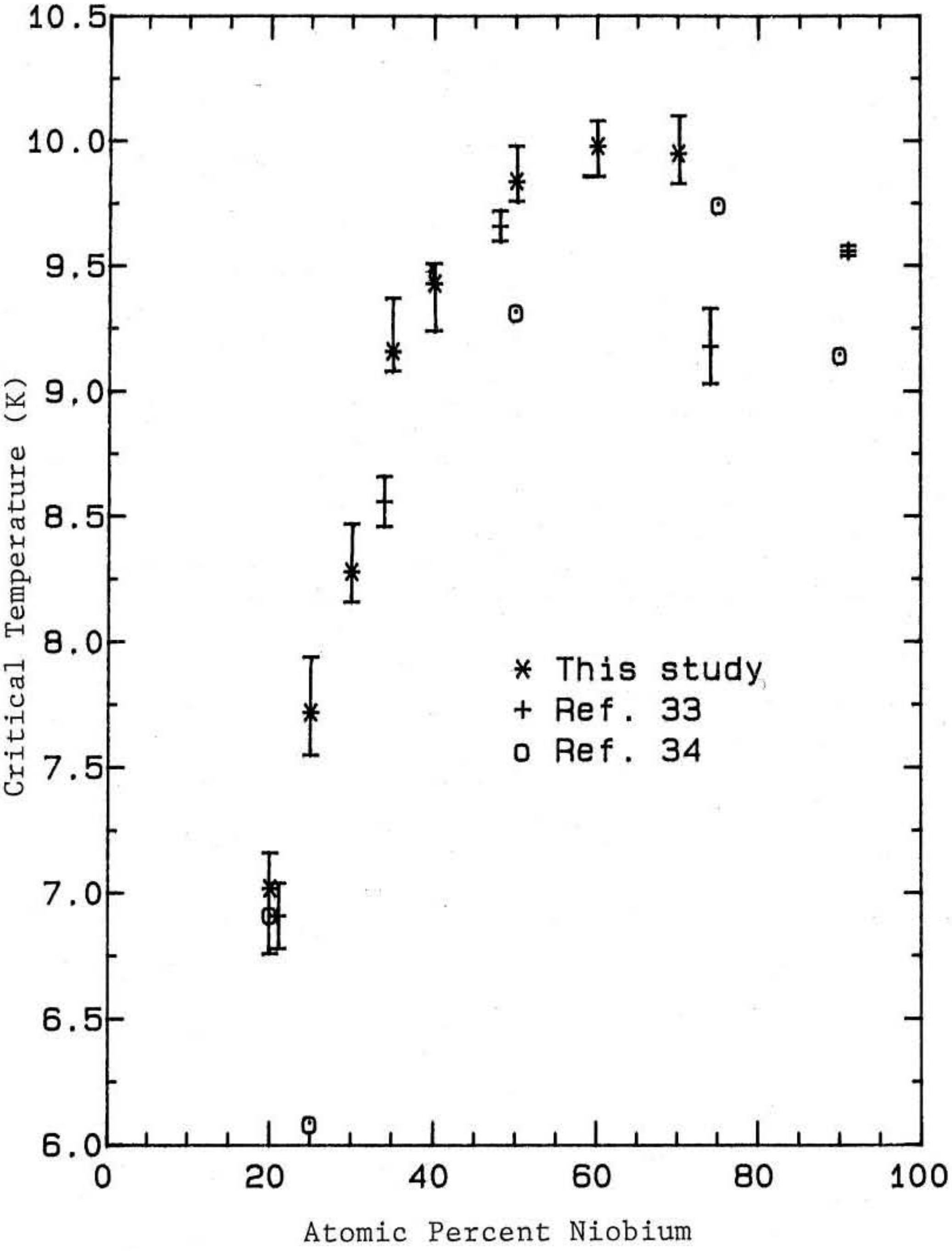

Figure 17: Calorimetric Transition Temperature Comparison

is definitely smaller for the Ti35at.%Nb and higher Nb alloys, seldom being more than 0.1K. The disagreement between different measures in this study is much less than the disagreement from one study to another, as can be seen by comparing the spread of data in figure 14 to that in table 2. This indicates that the discrepancies between studies are real, the result of differences in microstructure rather than measurement technique.

9 Extraction of γ and θ_d

The standard way to analyze heat capacity data relies on the Debye model for lattice specific heat. Using this model, in addition to the free electron model for conduction electrons in a metal, it is possible to approximate the material's heat capacity as follows:

$$C(mJ/molK^2) = \gamma T + \frac{1.944 \times 10^6}{\theta_d^3} T^3 \tag{12}$$

Here, θ_d is the Debye temperature and γ the electronic specific heat coefficient. This last quantity can be related to the electronic density of states at the Fermi surface (if the surface is spherical) in the following way:

$$n(\epsilon_f) = \frac{3}{k_b^2 \pi^2} \gamma \tag{13}$$

Based on this model, a plot of C/T versus T^2 should give a straight line with

% Nb	resistive	inductive	H_{c_2} extrapolation	calorimetric
20	7.2±.02	7.08±.04	7.19±.05	$7.02^{+.14}_{-.26}$
25	8.39±.09	$7.63^{+.06}_{-.09}$	8.27±.09	$7.72^{+.22}_{-.17}$
		$8.06^{+.10}_{-.13}$		
30	8.91±.03	$8.70^{+.13}_{-.21}$	8.71±.05	$8.28^{+.19}_{-.12}$
35	9.16±.02	8.97±.05	9.07±.05	$9.16^{+.21}_{-.08}$
40	9.47±.08	9.28±.08	9.23±.05	$9.43^{+.08}_{-.19}$
50	9.71±.03	9.67±.06	9.47±.02	$9.84^{+.14}_{-.08}$
60	9.94±.01	9.81±.06	9.88±.02	$9.98^{+.10}_{-.12}$
70	10.00±.01	9.88±.07	9.86±.02	$9.95^{+.15}_{-.12}$

Table 2: Comparson of Critical Temperatures

y-intercept γ and slope related to θ_d.

The separation technique outlined above is complicated somewhat in superconductors. In these materials, conduction electrons condense into Cooper pairs at temperatures below the critical temperature, so the heat capacity of the electron gas is dramatically altered. Without the benefit of low temperature normal state data, the extrapolation to 0K is susceptible to error. For the high niobium alloys the problem is greatest, because the higher critical temperatures prevent a wide range of normal state measurements. The errors in the specific heat data are magnified by the extrapolation process, so that a 3% error in C leads to a 12% error in γ if the lower limit of data used is about 9K. Specific heat data for the alloys in this study are presented in figures 18 through 25, along with the Debye extrapolation of that data.

In table 3 the γ and θ_d values for each composition are listed. These are based on a linear, least squares fit to the data between T_c and 12K, with the errors given by the coefficient uncertainty of the fit. Included in the table are entries for pure niobium, based on measurements made on the high purity niobium sample described on page 36. These values are within 2% of those derived by Leupold and Boorse[35](γ=7.38 mJ/mol-K^2, $\theta_d = 241K$) from data over the same temperature range.

The data shows a general trend by which γ increases from 5.1 mJ/mol-K^2 at 20at.%Nb to a peak of 8.6 mJ/mol-K^2, then declining towards the pure Nb

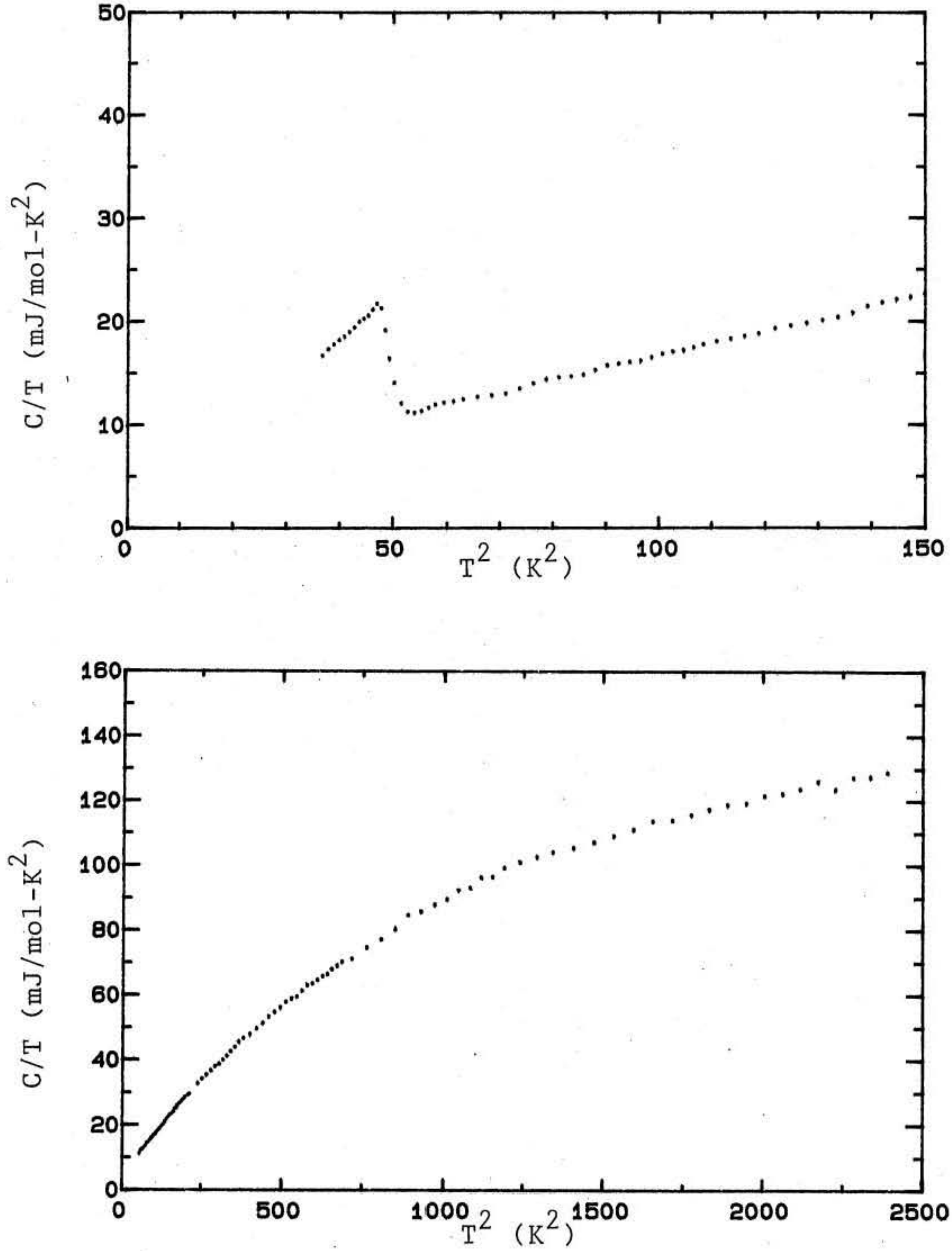

Figure 18: Debye Plots For 20% Niobium Alloy

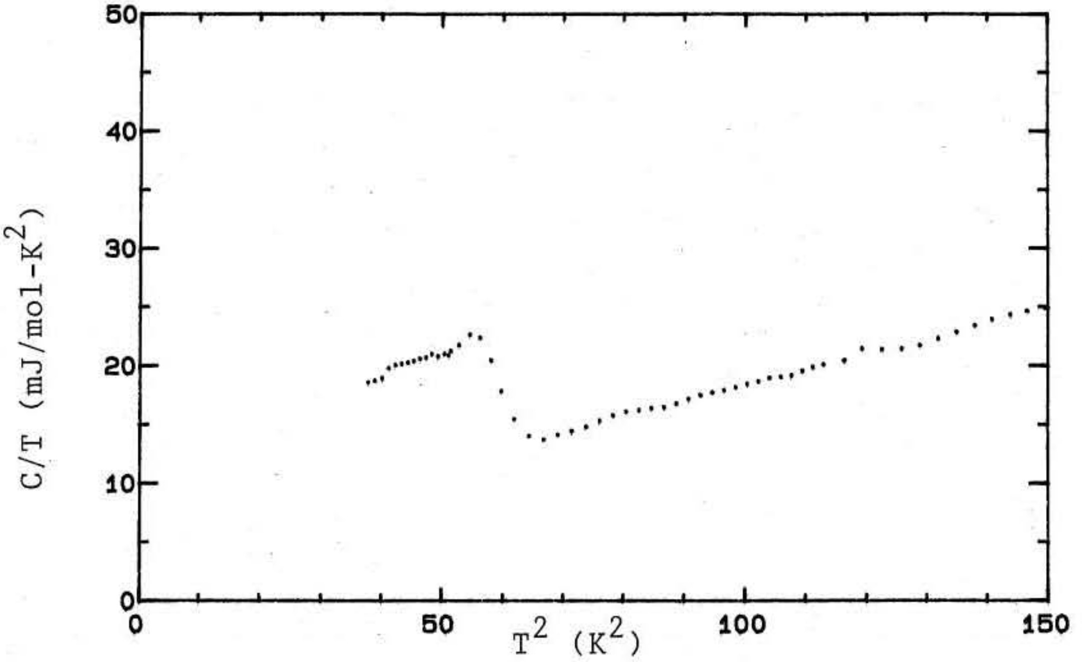

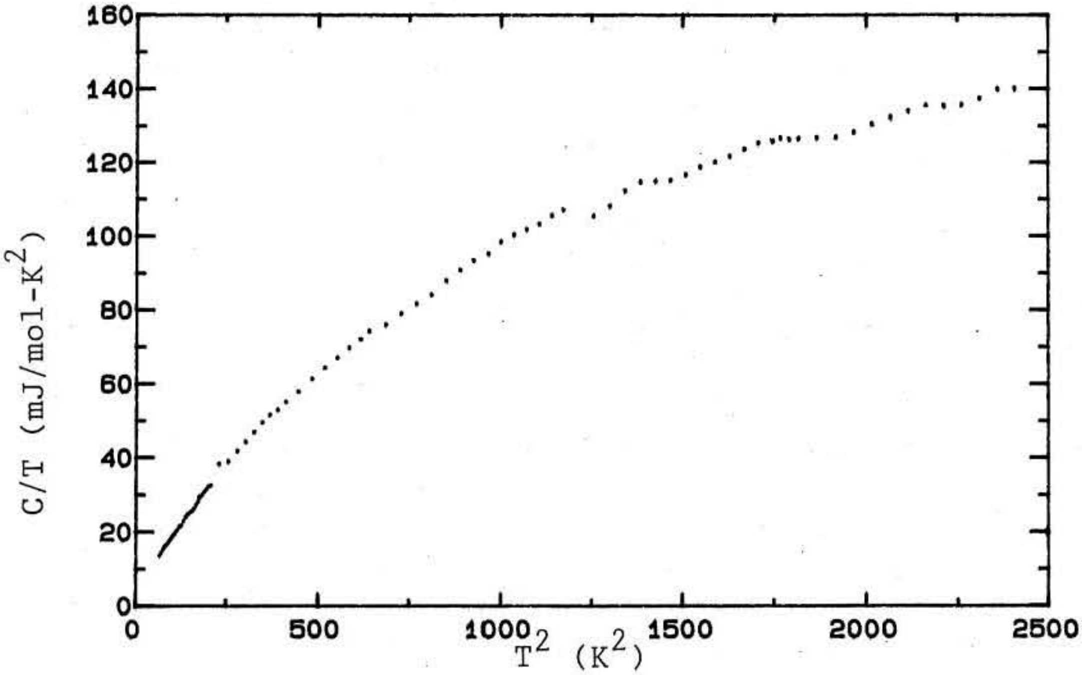

Figure 19: Debye Plots For 25% Niobium Alloy

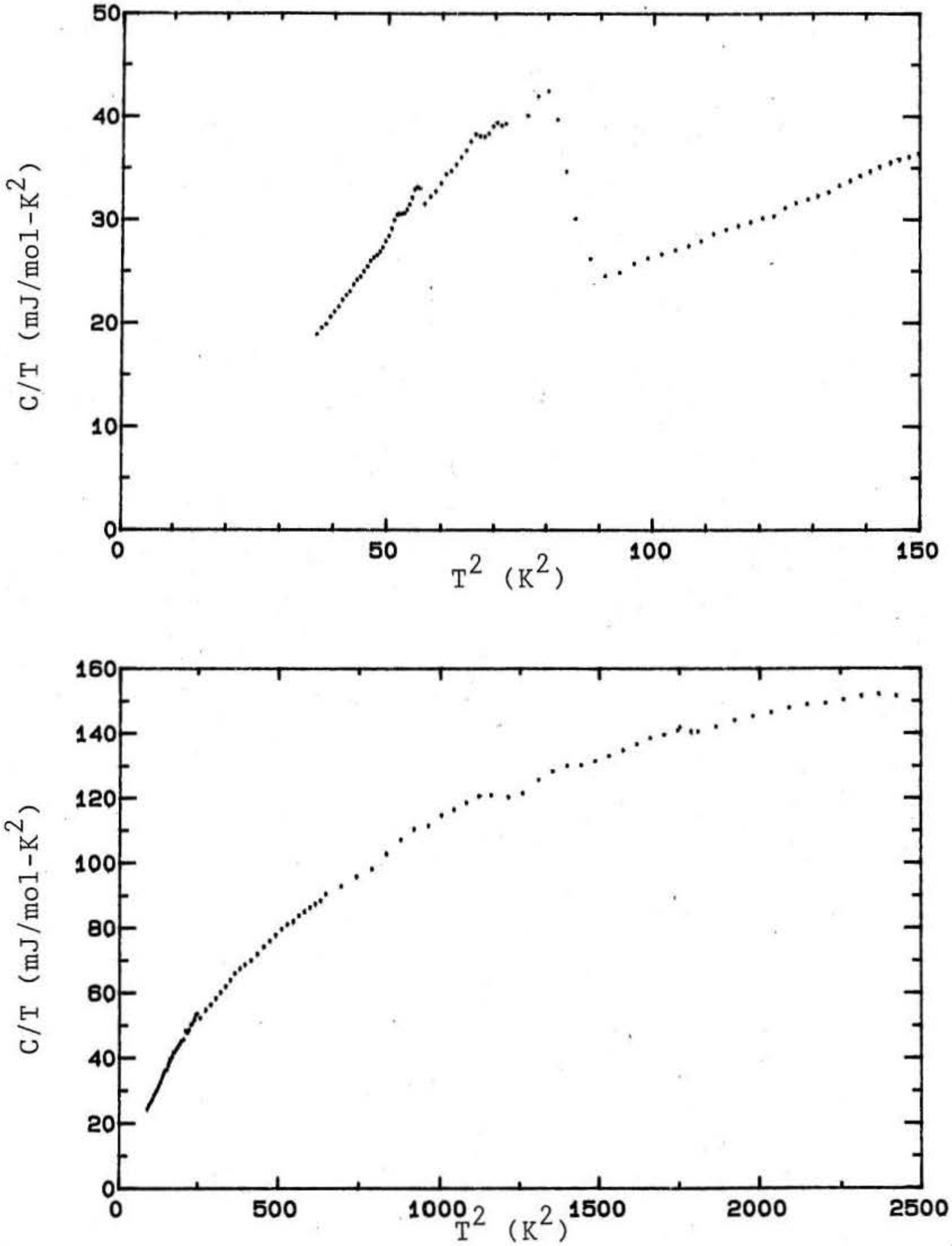

Figure 21: Debye Plots For 35% Niobium Alloy

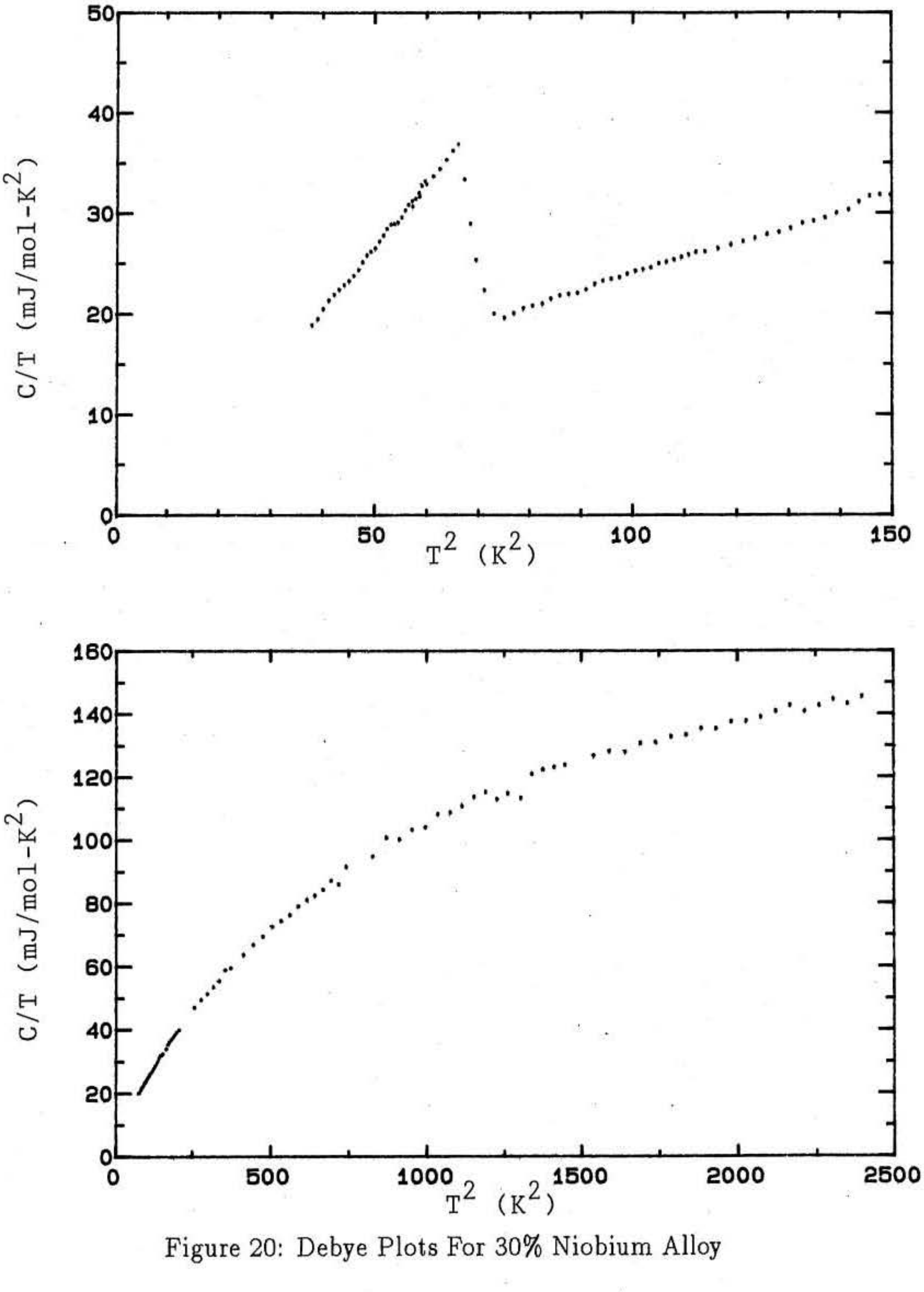

Figure 20: Debye Plots For 30% Niobium Alloy

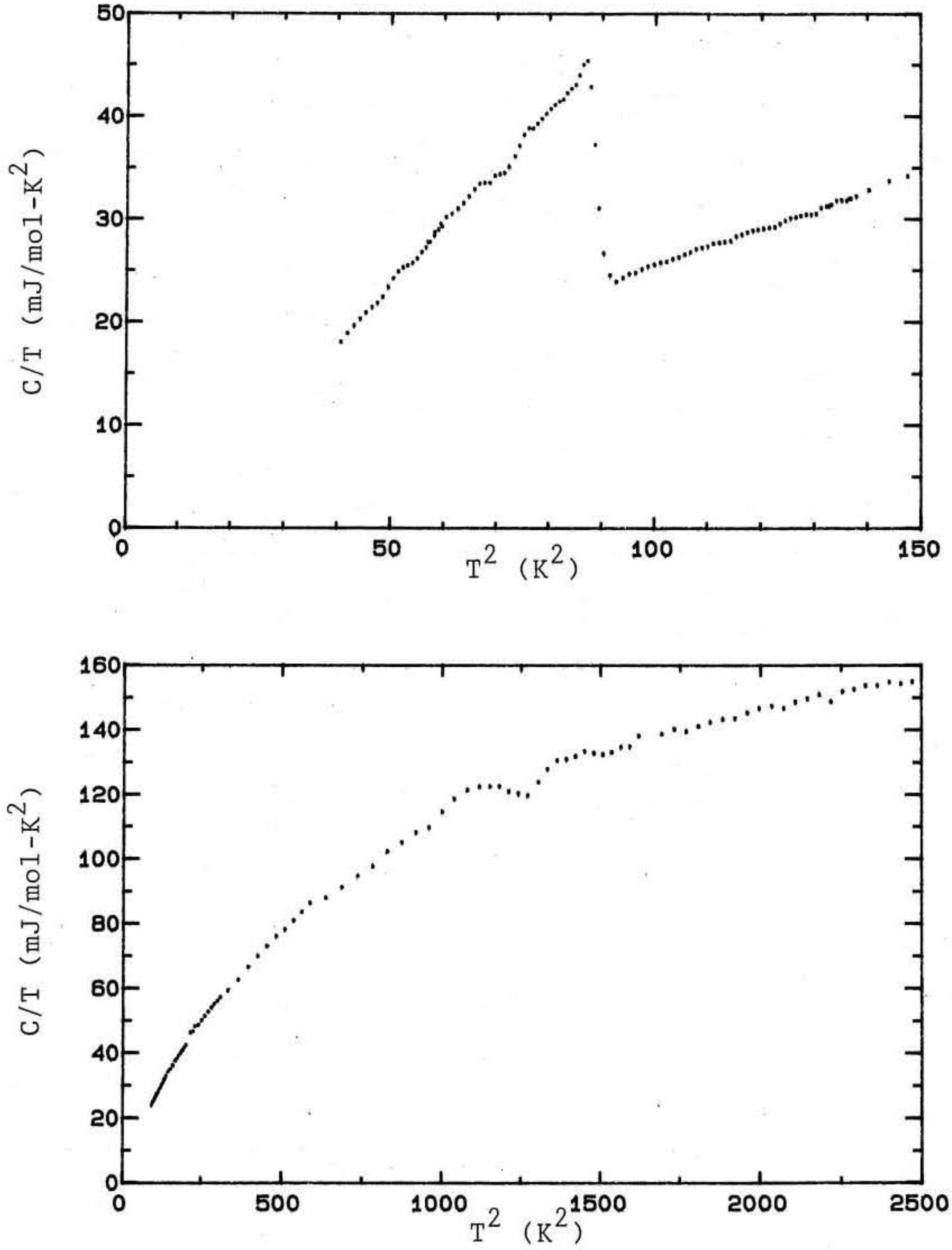

Figure 22: Debye Plots For 40% Niobium Alloy

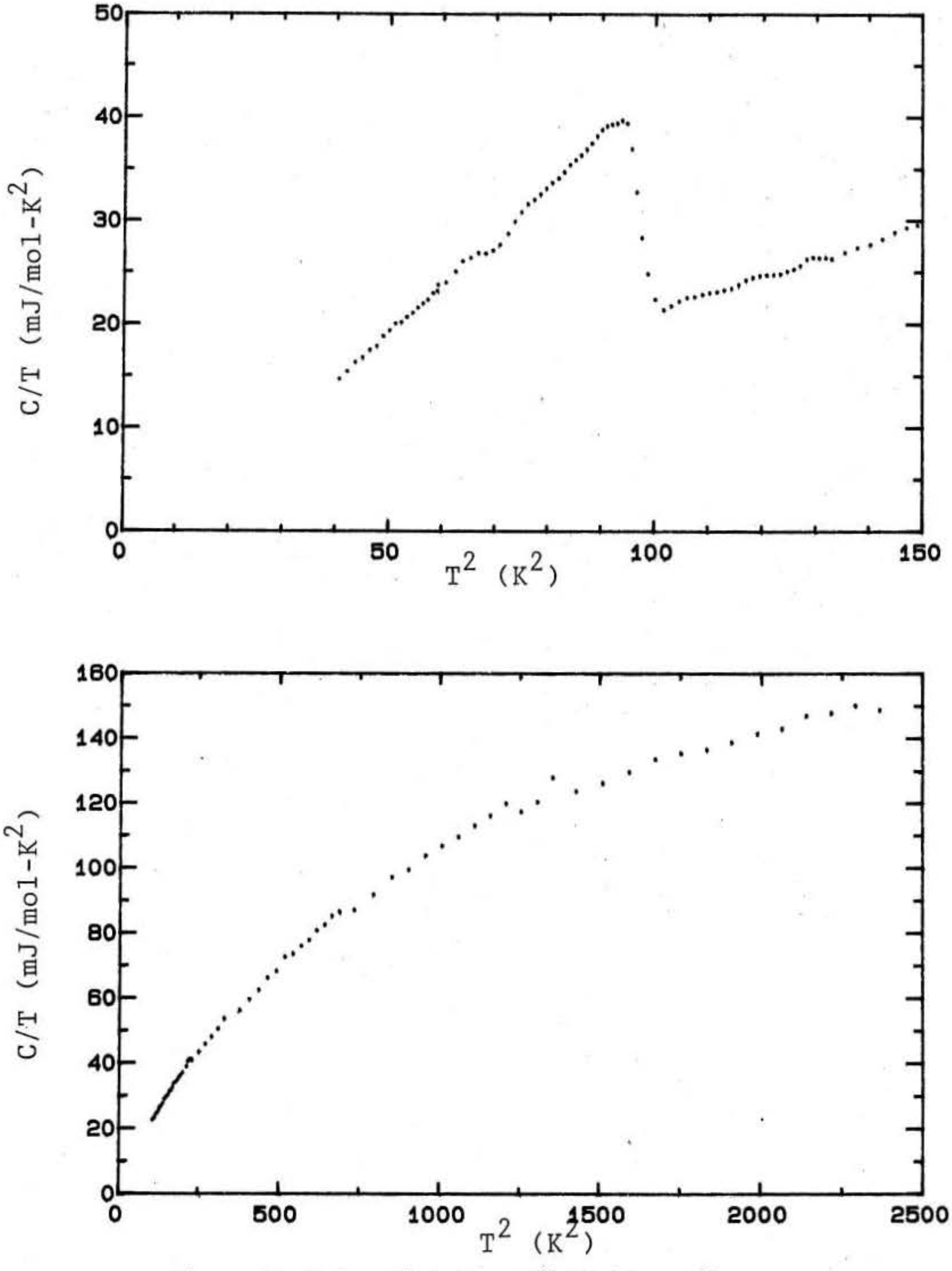

Figure 23: Debye Plots For 50% Niobium Alloy

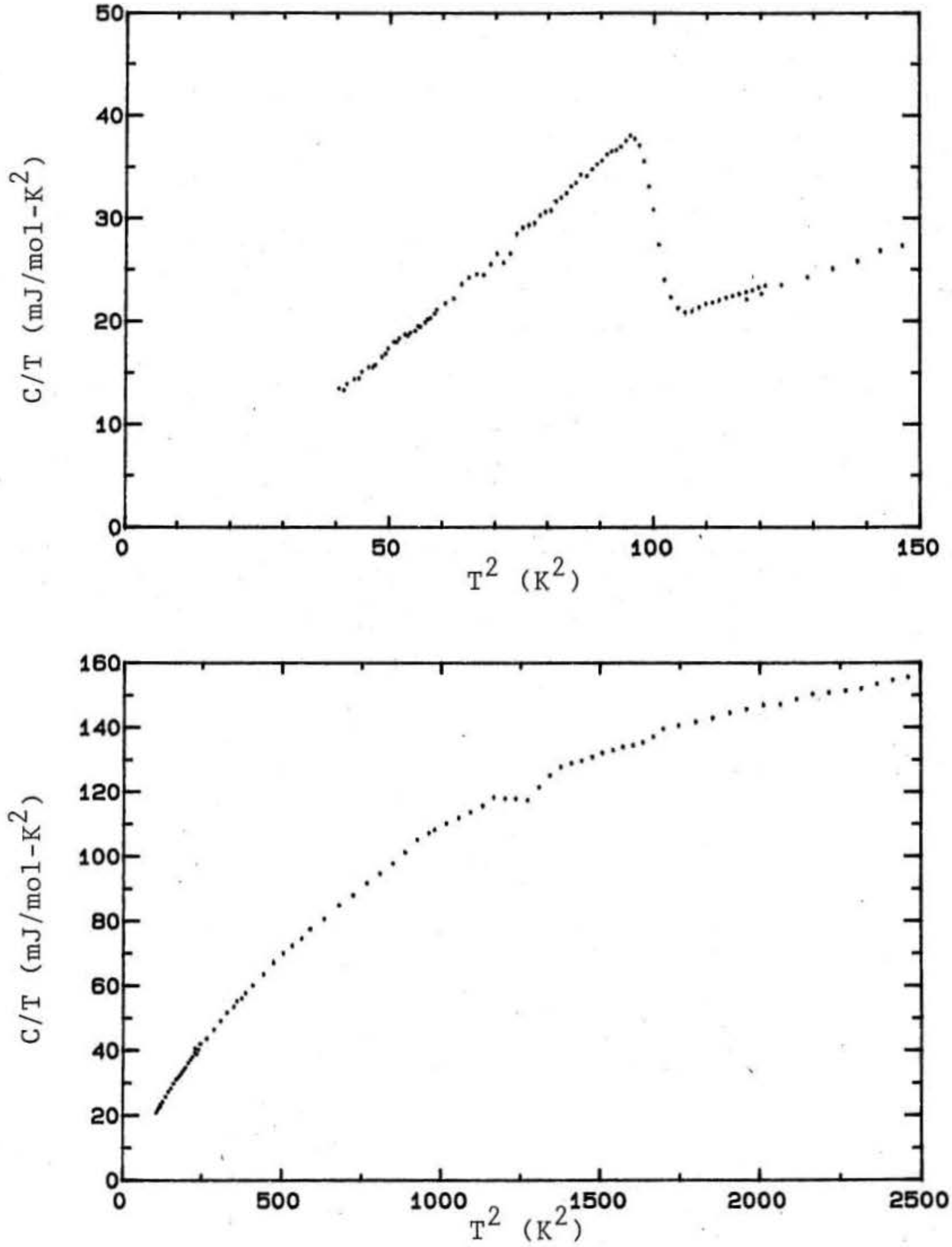

Figure 24: Debye Plots For 60% Niobium Alloy

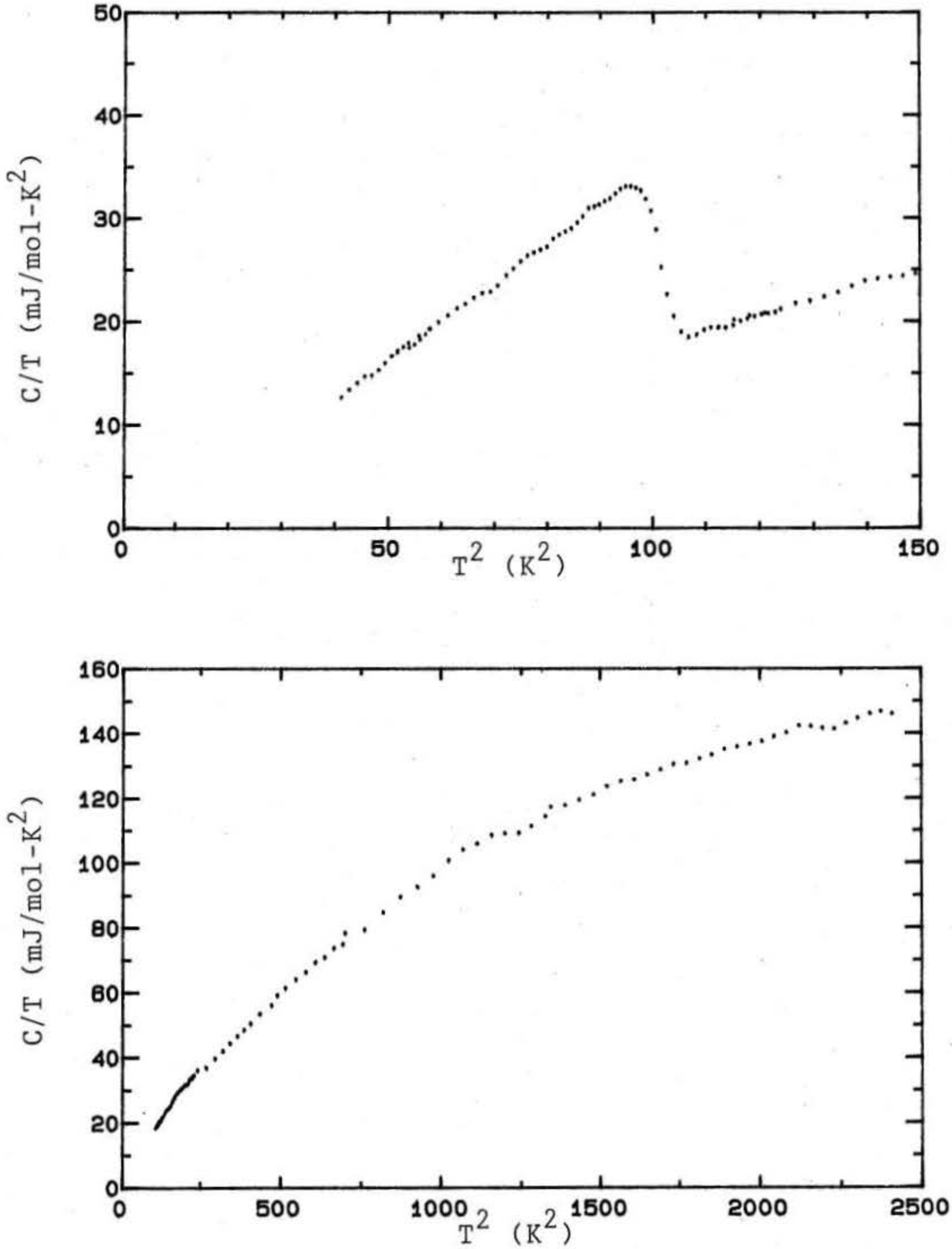

Figure 25: Debye Plots For 70% Niobium Alloy

% Niobium	γ(mJ/mol-K^2)	θ_d(K)
20	5.1±.2	255
25	5.5±.4	247
30	8.6±.5	233
35	6.3±1.0	213
40	8.2±.8	224
50	5.6±1.1	231
60	4.2±2.2	231
70	3.2±1.3	237
100	7.4±.4	243

Table 3: γ and θ_d Values

value of 7.4 mJ/mol-K^2. θ_d follows a similar but inverse trend, starting at 255K (20at.%Nb), reaching a minimum of 213K at 35at.%Nb, and climbing to 243K at pure Nb. The trend of θ_d is relatively smooth, but this is not the case for the γ values. The 35at.%Nb value is anomalously low, and the steady decline in γ from 40at.%Nb to 70at.%Nb (8.2 to 3.2 mJ/mol-K^2) requires a significant upturn beyond 70at.%Nb in order to reach the pure Nb value.

In figures 26 and 27, the Nb-Ti alloy results are plotted against those measured by Sasaki[33] and by Savitskii et. al.[34], as well as some recent, unpublished work by Ho[36]. The great scatter in these data is unsatisfactory, making it impossible to come to firm conclusions concerning the behavior of γ across the alloy system. In the data of Savitskii et al., which was for years the only data available, γ ranges from 9.2 mJ/mol-K^2 (20at.%Nb), rises to 10.5 (50at.%Nb), then declines slowly to about 10.2 mJ/mol-K^2 (75, 90at.%Nb). The four data points of Ho are closely spaced from 28 to 37at.%Nb and show γ increasing sharply from 8 to 11 mJ/mol-K^2. These data, as well as those of Sasaki, are all higher than the data taken in the present study.

One concern about treating the data within the Debye formalism is that the C/T versus T^2 plot exhibits some curvature, as can be seen by examining the high temperature Debye plots exhibited in figures 18 through 25. Because of this curvature, the y-intercept of any linear fit to the data will systematically increase as the temperature range of the fit is increased. The data for 20, 25, and 30at.%Nb

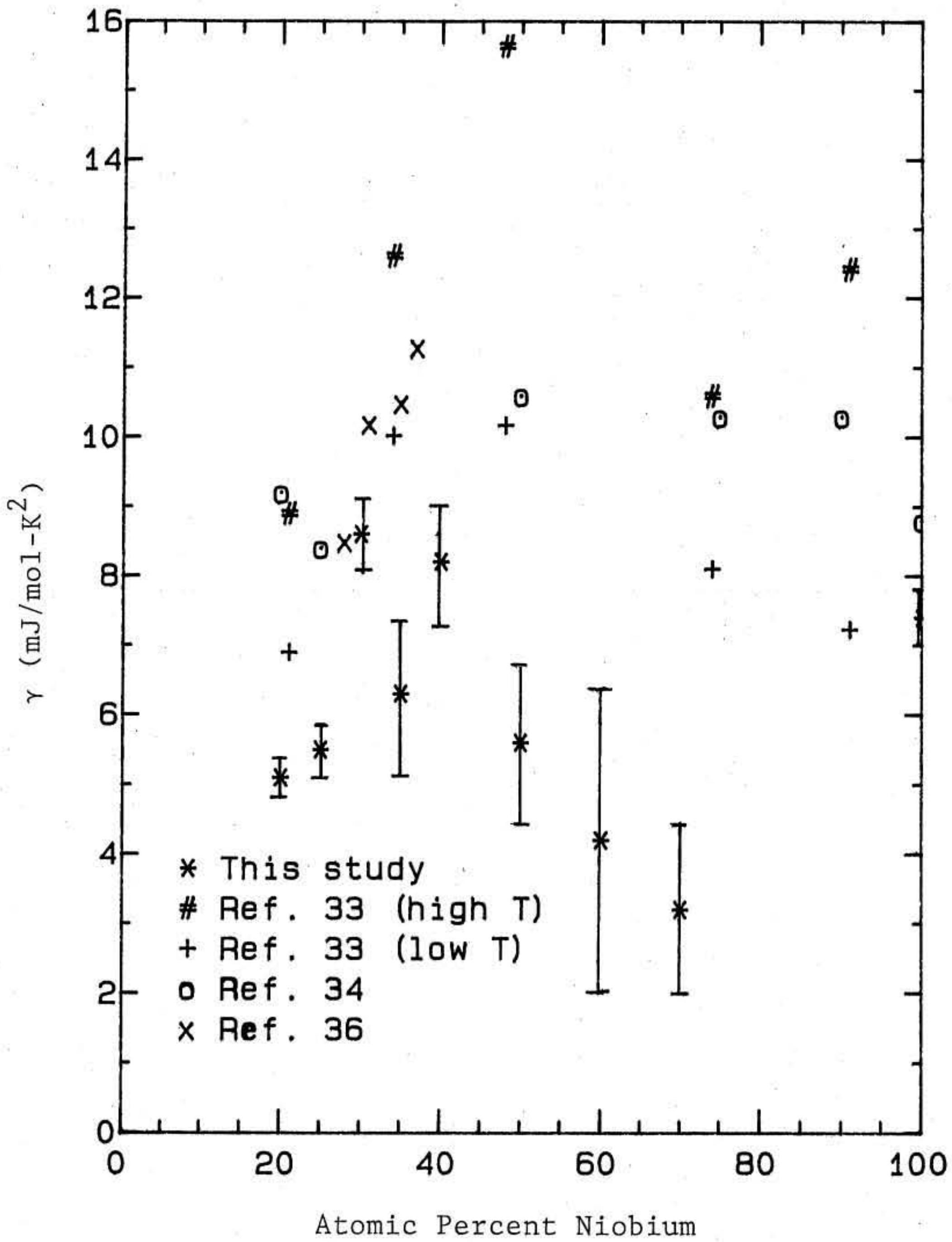

Figure 26: Comparison of Extrapolated γ Values

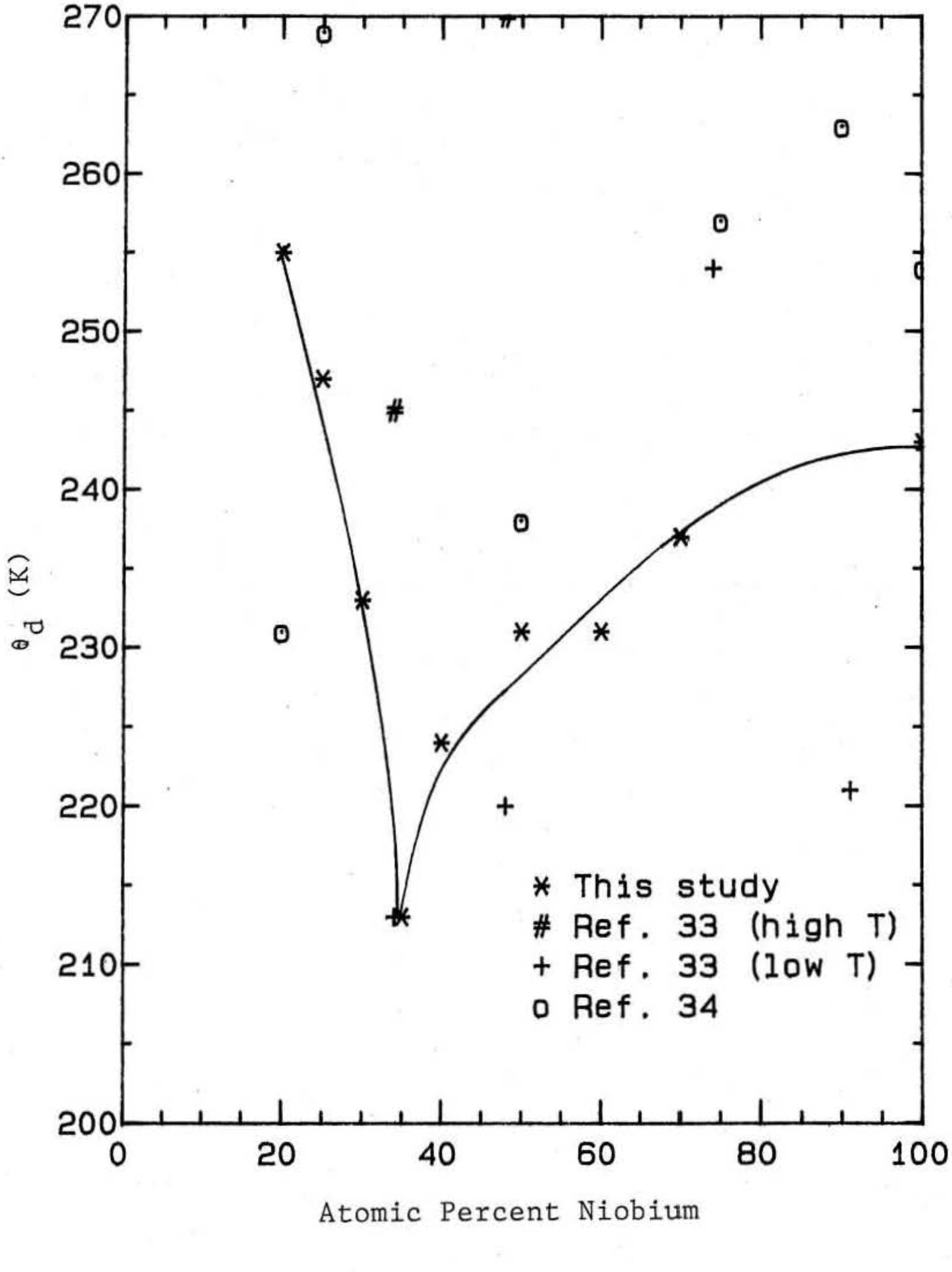

Figure 27: Comparison of Debye Temperatures

are not greatly affected by this curvature; extending the upper limit of the fit from 12K to 16K only increases the γ values by a few percent. In contrast, the γ value for 35at.%Nb is increased 30% by the same change in temperature range. The T_c-16K based γ extrapolation for 40at.%Nb is 10% higher than that based on T_c-12K data, for 50 and 60at.%Nb the increase is 20%, and for 70at.%Nb, the increase is over 60%. Clearly, the range of data used can have a large effect on extrapolated γ values for these alloys, but there is no precise way of determining the correct range. Since the Debye model is most reliable at low temperatures, and because of noticible curvature of the Debye plots, only the lowest temperature extrapolations (T_c-12K) will be used.

Another of the difficulties involved in extracting reliable γ values is illustrated in the work of Sasaki[33], where, for a variety of compositions, the normal state Debye plots exhibit a kink at low temperatures. These measurements, made in a magnetic field in order to depress T_c, show a clear change in slope of the Debye plot at a temperature which varies with composition from about 6K to 8K. Extrapolations based on data below this kink temperature (designated "low T" data in figure 26) lead to values of γ much lower than those derived from higher temperature data (designated "high T" data). A similar anomaly has been noticed in pure niobium[35], but the direction of the kink was the opposite of that found by Sasaki, so the effect was to elevate, rather than depress, the 0K intercept of the Debye plot.

Since superconductivity is an ordered electronic state, there is no latent heat of transformation to the normal state, in the absence of a magnetic field. This means that the entropy of the normal state and the superconducting state are equal at the critical temperature, and this fact can be used to check the consistency of the extrapolated normal state data. The entropy of the superconducting state can be obtained by integrating the function C/T from 0K to T_c. Since no data is available at temperatures below about 6K, it is assumed that C/T is proportional to T^2 and goes to 0 at 0K. As can be seen in figures 18 through 25, this assumption is reasonably accurate. In any case, the higher temperature region (where data is available) weighs more heavily in the entropy integral. Roughly speaking, the total error in the calculation should be less than 10%. The entropy of the normal state can be determined by integrating the Debye equation up to T_c. These two entropies, S_s and S_n, are listed in table 4.

The agreement between S_s and S_n is satisfactory for 5 samples (20, 25, 30, 40, and 100at.%Nb) but less good for 4 (35, 50,60, 70at.%Nb) where S_s-S_n is of order 20-30% of S. In the latter cases, S_n is significantly lower than S_s. Whether this is because the Debye extrapolation does not accurately model the low temperature behavior of these samples, or because there are errors in the experimental data is not clear. An upward kink in the normal state heat capacity below T_c, such that γ was higher than expected, would reduce this discrepancy, but only calorimetry in a magnetic field can generate the data necessary to verify this.

% Niobium	S_s(mJ/mol-K^2)	S_n	S_s-S_n
20	51.4±5.1	48.6±1.4	2.8±6.5
25	68.7±6.9	62.3±3.1	6.4±10
30	98.2±9.8	100.3±4.1	-2.1±13.9
35	137.3±13.7	108.9±9.2	28.4±22.9
40	133±13.3	126±7.5	7±20.8
50	124.7±12.5	105.3±10.8	19.4±23.3
60	119.5±12	94.2±22	25.3±34
70	108.6±10.9	79.6±12.9	29±23.8
100	98.3±9.8	104±3.7	-5.7±13.5

Table 4: Entropies at T_c of Normal and Superconducting State

10 GLAG Predictions

According to the GLAG theory[37], there is a relationship between the normal state resistivity, electronic density of states, and dH_{c_2}/dT for a superconductor. The equation is as follows:

$$dH_{c_2}/dT|_{T_c} = 4485\gamma\rho \qquad \text{(MKS)} \tag{14}$$

Using this equation, it is possible to predict γ from resistivity and H_{c_2} data. Figure 28 presents a comparison of the GLAG prediction of γ to the value determined using a Debye extrapolation. The agreement between these values is quite rough, and particularly poor in the high niobium alloys. There, the GLAG equation predicts that γ should increase slowly as niobium concentration increases, while the Debye extrapolation implies that γ decreases substantially over the same range.

11 WHH Theory

The WHH theory of H_{c_2} is based on a gauge invariant solution of the linearized Gorkov equation for the superconducting gap energy[1]. there are two fundamental parameters in the theory; α the paramagnetic limitation parameter, and λ_{so} the spin-orbit scattering parameter. These are defined as follows:

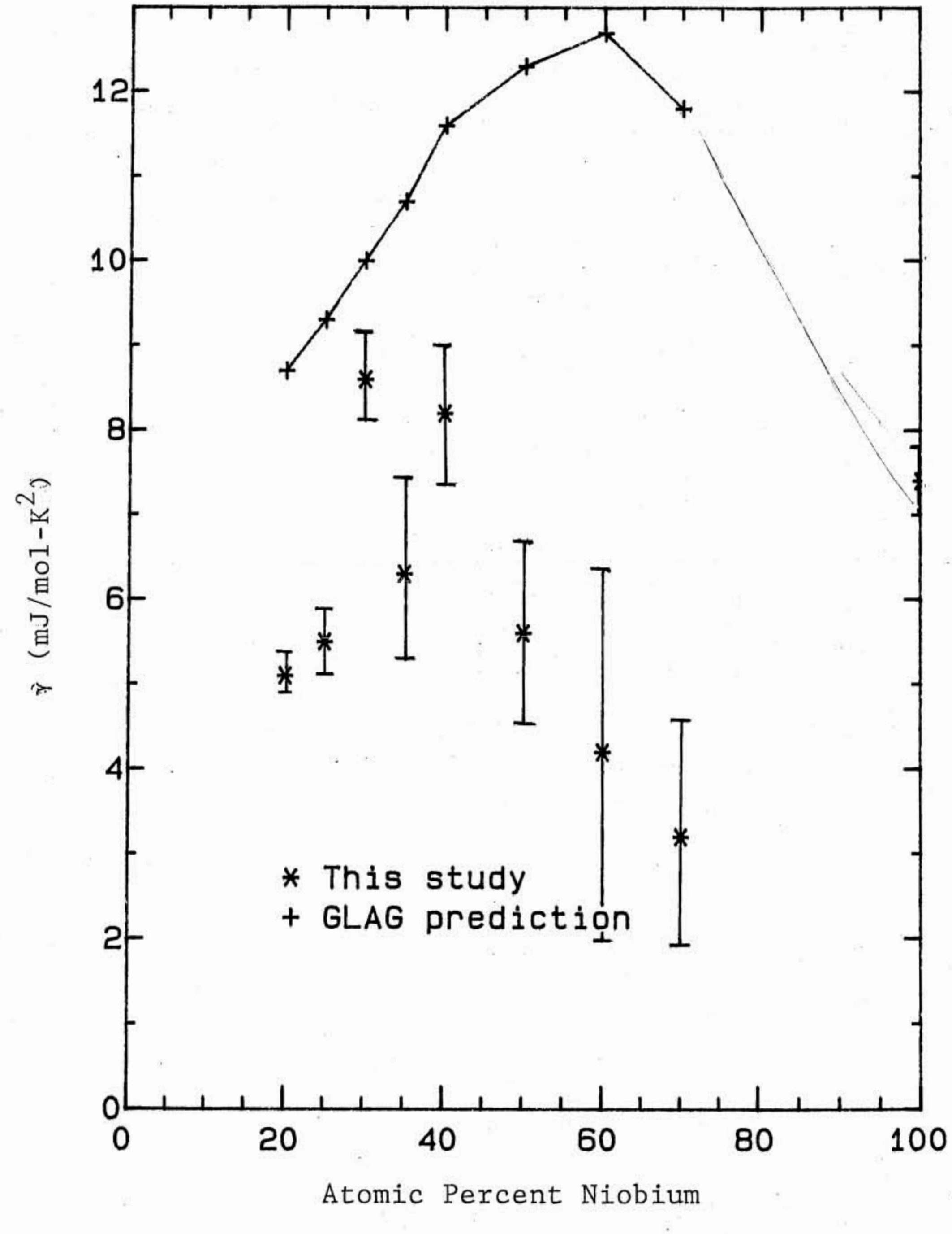

Figure 28: Comparison of GLAG Prediction and Debye Extrapolation

$$\alpha = \frac{3h}{4\pi m v_f^2 \tau} \qquad \text{(CGS)} \tag{15}$$

$$\lambda_{so} = \frac{2h}{6\pi^2 k_b T_c \tau_{so}} \qquad \text{(CGS)} \tag{16}$$

Here, m is the electron mass, v_f is the Fermi velocity, τ is the transport scattering time, T_c is the critical temperature, and τ_{so} is the time between scattering events which allow electron spin flips. Additionally, the variables of magnetic field and temperature are converted to reduced variables using these definitions:

$$\bar{h} = \frac{2ev_f^2\tau}{6\pi c k_b T_c} H_{c_2} \qquad \text{(CGS)} \tag{17}$$

$$t = T/T_c \tag{18}$$

Though the derivation is carried out for arbitrary mean free path, this general equation cannot be solved analytically. The most often quoted and used formulation is valid only in the limit of short mean free path, and is expressed as follows:

$$\begin{aligned} \ln t &= \Psi(1/2) - \left[\frac{1}{2} + \frac{\lambda_{so}}{8X}\right] \Psi\left[\frac{1}{2} + \frac{Y-X}{t}\right] - \left[\frac{1}{2} - \frac{\lambda_{so}}{8X}\right] \Psi\left[\frac{1}{2} + \frac{Y+X}{t}\right] \\ X &= \sqrt{(\lambda_{so}/4)^2 - (h\alpha/2)^2} \\ Y &= (h/2) + (\lambda_{so}/4) \end{aligned} \tag{19}$$

The digamma function, $\Psi(x)$ is a standard function, defined as the logarithmic derivative of the gamma function. The restriction on mean free path is simply that $k_bT_c \ll h/2\pi\tau$. An additional restriction is placed on one integral in the general equation, but the physical significance of this restriction is not obvious. An appendix to the WHH paper shows that the restriction can be satisfied when $\tau \ll \tau_{so}$ if the effects of orbital diamagnetism are ignored, but it is not clear whether or not it can be satisfied for larger spin-orbit scattering rates.

There are a few assumptions built into the WHH theory by virtue of its reliance on the Gorkov equation. The first of these is that the Fermi surface is spherical, so that the use of an average Fermi velocity is physically sensible. The next is that the scattering of quasi-particles can be described with a classical approach, and their trajectories are not affected by the applied magnetic field between scattering events. This is satisfied if $(eh/2\pi m) \ll k_bT_c + h/2\pi\tau$. The scattering centers must be dilute and uncorrelated, that is, they must act independently, so that the aggregate effect of these scatterers is simply the sum of their individual effects. Only the most likely types of scattering events are considered, so it is assumed that all others have negligible probability of occurance. The probability of these unlikely events is estimated by Gorkov[38], and he states that they should be unimportant if $k_f\ell \gg 1$. This restriction is not exact, but rather gives a general idea of the range of applicability of the equation. Finally, two assumptions are made about the phonon mediated attraction between electrons. One is that the Coulomb repulsion between electrons is screened by the electron gas, and that the screening is static, i.e., it can be treated using a psuedopotential in place of the Coulomb potential.

The other assumption is that the strength of the attractive interaction does not depend on the energy or wavevector of the phonon intermediary.

As a practical equation, the form quoted in equation 19 has some drawbacks, since all the parameters are determined by microscopic quantities, such as v_f and τ. However, in the limit $t \rightarrow 1$, $d\bar{h}/dt$ for this equation equals a constant, $4/\pi^2$. Experiments indicate that superconductors exhibit constant dH_{c_2}/dT near T_c, so it is usual, and indeed recommended in the WHH paper, to define an empirical reduced field h, such that:

$$\left.\frac{dh}{dt}\right|_{t\rightarrow 1} = \left.\frac{d\bar{h}}{dt}\right|_{t\rightarrow 1} \tag{20}$$

Thus:

$$h = \frac{4H_{c_2}}{\pi^2 (dH_{c_2}/dT)|_{T_c} T_c} \tag{21}$$

If we compare equations 17 and 21 we find that:

$$\bar{h} = \frac{2ev_f^2\tau}{6\pi c k_b T_c} H_{c_2} = \frac{4H_{c_2}}{\pi^2 (dH_{c_2}/dT)|_{T_c} T_c} \qquad \text{(CGS)} \tag{22}$$

Or, rearranging into SI units:

$$v_f^2 \tau = \frac{3.29 \times 10^{-4}}{dH_{c_2}/dT|_{T_c}} \qquad \text{(MKS)} \tag{23}$$

Thus, the paramagnetic limitation parameter becomes:

$$\alpha = \alpha_s = .528 dH_{c_2}/dT|_{T_c} \qquad \text{(MKS)} \tag{24}$$

Another way to link the WHH parameters to macroscopic quantities is through the Boltzmann equation:

$$\rho = \frac{6\pi^2 h}{e^2 v_f \tau S} \qquad \text{(MKS)} \tag{25}$$

Here, ρ is the resistivity and S is the Fermi surface area, which is proportional to conduction electron density. this equation is valid for systems with a spherical Fermi surface in which only elastic scattering occurs. The first assumption is already required by the WHH derivation, so only the second is an additional constraint. the Boltzmann equation alone is not useful, since although it relates v_f and τ to ρ, a measureable quantity, it also introduces another microscopic parameter, S. To eliminate S, it is helpful to use specific heat information. Recall that the low temperature heat capacity of a free electron gas is related to the electronic density of states in that material as follows:

$$\gamma = \frac{n(\varepsilon_f) k_b^2 \pi^2}{3} \tag{26}$$

In this equation, $n(\varepsilon_f)$ is the Fermi surface density of states and γ the proportionality constant of that part of the specific heat which depends linearly on temperature. Since the Fermi surface area ,S, is equal to $4\pi k_f^2$, and $n(\varepsilon_f)$ equals

$4mk_f/h$ for a spherical Fermi surface, this can be reexpressed:

$$\gamma = \frac{k_b^2 S}{6hv_f} \tag{27}$$

If this equation is combined with equation 25, the result is as follows:

$$v_f^2\tau = 7.33 \times 10^{-8}/\gamma\rho \qquad \text{(MKS)} \tag{28}$$

This relation can be used along with the definition of $\alpha$to give:

$$\alpha = \alpha_n = 2368\gamma\rho \qquad \text{(MKS)} \tag{29}$$

These calculations show that there are two methods for determining α, either using equation 24 or equation 29. The first of these is refered to as α_s, the paramagnetic limitation parameter determined from superconducting measurements, while the second is labled α_n, since it is derived from normal state measurements.

12 Extension of the WHH Treatment

The results above come from a nearly free electron model of the superconductor, where the electron-phonon interaction simply provides an effective potential in which the electron moves. Such a one electron treatment neglects many body interactions, but it is possible to include some of these effects in the context of the WHH theory. According to Migdal[39], perturbation theory can accurately account for the time dependence of the electron-phonon interaction, and this effect can be incorporated into the WHH formalism through the use of a renormalized electron mass. This renormalization factor, $1 + \lambda_{ep}$, is given by the following integral[40]:

$$\lambda_{ep} = 2 \int_0^{\infty} \alpha^2(\omega) F(\omega) d\omega / \omega \tag{30}$$

Here, $\alpha^2(\omega)$ is the electron-phonon interaction matrix element and $F(\omega)$ is the phonon density of states. According to Grimvall[41], renormalization affects microscopic properties in the following way, with starred quantities representing renormalized variables:

$$\begin{aligned} m^* &= m(1+\lambda_{ep}) && (31) \\ \tau^* &= \tau(1+\lambda_{ep}) && (32) \\ v_f^* &= v_f/(1+\lambda_{ep}) && (33) \end{aligned}$$

Dimensional analysis of α,from equation 15, shows that it is invariant under this electron-phonon renormalization, i.e., $\alpha(m,v_f,\tau) = \alpha(m^*,v_f^*,\tau^*)$. Since v_f and τ are determined from experimental quantities, either through equations 23 or 28, they are renormalized quantities. This means that to get correct values of α, the renormalized electron mass, m^*, must inserted into equations 24 and 29, so that:

$$\alpha_s = \frac{.528}{1+\lambda_{ep}} \left. \frac{dH_{c_2}}{dT} \right|_{T_c} \tag{34}$$

$$\alpha_n = \frac{2368}{1+\lambda_{ep}}\gamma\rho \tag{35}$$

It is possible to determine λ_{ep} using one of two schemes. The first involves measuring a quantity affected by the electron-phonon renormalization, such as the specific heat at low temperature, and comparing it to the value predicted by band structure calculations. Unfortunately, band structure calculations for solid solution alloys are complicated, and have not been done for Nb-Ti. Thus, for the Nb-Ti system, this first approach is unhelpful. Another, more indirect technique makes use of one of the many equations relating T_c to electron and phonon parameters of a material. One of these theories, proposed by Allen and Dynes[42] states that T_c is given by:

$$T_c = \frac{\omega_\ell}{1.2}\exp\frac{-1.04(1+\lambda_{ep})}{\lambda_{ep}-\mu^*(1+.62\lambda_{ep})} \tag{36}$$

Here, μ^* is a Coulomb pseudopotential and ω_ℓ is an average phonon frequency defind as:

$$-\log\omega_\ell = \frac{\int\alpha^2(\omega)F(\omega)\ln\omega d(\ln\omega)}{\int\alpha^2(\omega)F(\omega)d(\ln\omega)} \tag{37}$$

The development of the pseudopotential used in the theory above is the subject of some debate. It is one of the parameters in the Eliashberg gap equation, and constitutes an electron-electron renormalization factor analogous to the one used to treat the electron-phonon interaction, as outlined above. Though in principle it can be calculated, there is no adaquate perturbation treatment of the problem[40], so usually this parameter is extracted from analysis of tunnelling data[43]. McMillan[44] advanced qualitative arguements to show that, for most BCC elemental transition metals, μ^* should be .13. A later solution to the Eliashberg equation[45] tabulated tunnelling values of μ^*, as well as values resulting from numerical solutions to the gap equation. For many of the elements and alloys studied, there was only rough agreement between these two measures, perhaps to within 30 or 40 percent. Indium, tantalum, niobium, and lead all had values within 30% of the suggested .13, and the Pb-Bi and In-Tl alloy systems showed no systematic variation with composition. For the Nb25at.%Zr alloy, tunnelling measurements suggested $\mu^* \approx .1$, while gap equation solutions implied that .18 was the correct value. In summary, the determinants of μ^* are not well understood, and thus only approximate estimates can be made. For the purposes of this study, μ^* is set equal to .13, with a probable error of .03.

The extensions outlined above were used by Orlando et. al.[4][46] to analyze the H_{c_2} behavior of Nb_3Sn and V_3Si, which were not accurately described by the original WHH theory. The revised theory modeled the temperature dependence of H_{c_2} for V_3Si better than the original, and avoided the problem of unphysically large λ_{so} values in the description of Nb_3Sn. These studies also introduced some further renormalization parameters to account for the effects of spin waves and strong coupling, but they are not very important for the treatment of Nb-Ti. Thus, only corrections that can be incorporated into the parameters λ_{ep} and μ^* will be included in the present study.

At first glance, it seems that the Allen and Dynes T_c equation provides no help in evaluating the revised WHH expresions. Though it relates λ_{ep} to T_c, it also introduces other parameters; μ^*, which is known only approximately, and ω_ℓ, which depends on the same $\alpha^2F(\omega)$ function that λ_{ep} does. A close examination of the definition of ω_ℓ (equation 37) shows that while λ_{ep} depends directly on $\alpha^2(\omega)$, ω_ℓ contains this term in both numerator and denominator, so only the frequency dependence of this function need be considered. In developing their theory, Allen and Dynes assumed that $\alpha^2(\omega)$ was independent of frequency. They found that ω_ℓ calculated on this basis, in combination with measured T_c's, generated λ_{ep} values which agreed well with the few data available from tunnelling measurements. Later measurements on A15 compounds [47] indicated that agreement with tunnelling experiments was possible only if $\alpha^2 \propto 1/\sqrt{\omega}$. Other measurements on Chevrel phase materials[48] indicate that $\alpha^2 \propto 1/\omega$. The function seems to depend weakly on frequency, and generally to increase with decreasing frequency. It also seems to exhibit the same frequency dependence for an entire class of materials with the same crystal structure. Since the Nb-Ti system is a BCC metal, like many of the elemental materials studied by Allen and Dynes, it is assumed that α^2 is approximately constant.

The crux of these extensions of the WHH theory is the determination of the phonon density of states, $F(\omega)$. From this, and the assumed frequency dependence of α^2, it is possible to calculate ω_ℓ. This quantity, when used in the Allen and Dynes equation along with a measured T_c and an assumed μ^*, in turn defines λ_{ep}, which is used to renormalize the WHH paramagnetic limitation parameter.

13 The Harmonic Lattice Approximation

From the heat capacity data, it is clear that the Debye model does not well represent these alloys in the region above 15K, so another approach is needed to examine this high temperature data. A more general model of the thermal properties of a lattice treats it as an ensemble of harmonic oscillators. The heat capacity, in this harmonic approximation, is given by the integral:

$$C = 3R \int_0^\infty F(\omega) x^2 \frac{e^x}{(e^x - 1)^2} d\omega \qquad (38)$$

Subject to the condition:

$$\int_0^\infty F(\omega) d\omega = 1 \qquad (39)$$

In these equations, $F(\omega)$ is the phonon density of modes, x=ω/T, and both ω and T are expressed in Kelvins ($h = k_b = 1$). From this, Chambers[49] showed that a family of functions of the heat capacity are related to $F(\omega)$ as follows:

$$C = 3RT^{n+1} \int_0^{x_c} \frac{F(\omega)}{\omega^n} x^{n+3} \frac{e^x}{(e^x-1)^2} d(\ln x) \tag{40}$$

He showed that, though this integral cannot be solved analytically, it can be used to generate an approximation to the function $F(\omega)$ from data on heat capacity as a function of temperature. If the term $F(\omega)/\omega^n$ is treated as a set of discrete steps, constant over some range of frequencies, this equation becomes:

$$\frac{C}{T^{n+1}} = 3R \sum_{i=1}^{j} \left(\frac{F}{\omega^n}\right)_i \int_{x_{i-1}}^{x_i} x^{n+3} \frac{e^x}{(e^x-1)^2} d(\ln x) \tag{41}$$

$$\frac{C}{T^{n+1}} = 3R \sum_{i=1}^{j} g_i B_n(x_i, x_{i-1}) \tag{42}$$

Here, x_i are defined by the limit frequencies, ω_i, which subdivide the frequency spectrum, g_i are the discrete values of $F(\omega)/\omega^n$ over the range i, and B_n is simply a shorthand for the integral part of the equation above. This equation illustrates that the problem of determining the values g_i reduces to finding a least-squares fit to C/T^{n+1} using the basis functions B_n. Finding such a fit is mathematically possible for any value of n, but the accuracy and uniqueness of the fit depend on whether the basis functions are orthogonal or not. Since the definition of orthogonality for rational functions requires that there be no "overlap" of the functions, it is clear from figure 29 that the B_n functions are not the ideal sort to use as basis functions. The n=0 function has a full width at half maximum (in log space) of about 1.9. This means that each g_i value would have to span a range of about 4:1

in frequency ($x_i = 4x_{i-1}$) for the basis functions to be sufficiently independent to make the fitting process well behaved. If higher order B functions are used, this averaging range is reduced, but the functions narrow quite slowly with increasing n. In the interest of physical comprhensibility, this study will make use of the B_2 functions. They are sufficiently narrow to allow g_i averaging over just one octave ($x_i = 2x_{i-1}$), and represent the same spectrum, within each octave, as the Debye model. Using these specifications, the fitting equation is:

$$\frac{C(T)}{T^3} = 3R\sum_{i=1}^{j} g_i \int_{x_{i-1}}^{x_i} x^5 \frac{e^x}{(e^x-1)^2} d(\ln x) \tag{43}$$

The frequency bands are defined by the following limit frequencies:

$$\omega_0 = 1K \quad \omega_1 = 25K \quad \omega_2 = 50K$$

$$\omega_3 = 100K \quad \omega_4 = 200K \quad \omega_5 = 400K$$

The lowest energy spectral band in this model is not easily determined through the use of the fitting proceedure described above. This is because these phonon energies (below 20K) most strongly affect the heat capacity at temperatures about one fifth as high, as is expected, since the B_2 function peaks at x=4.93. However, since no data is available at such low temperatures, and since the coefficient of this lowest octave only weakly effects the data at higher temperatures that is available, this parameter is not freely varied, but rather fixed using a Debye extrapolation. This is possible if we compare the Debye integral to a form of equation 43 in the limit case i=1. These integrals are:

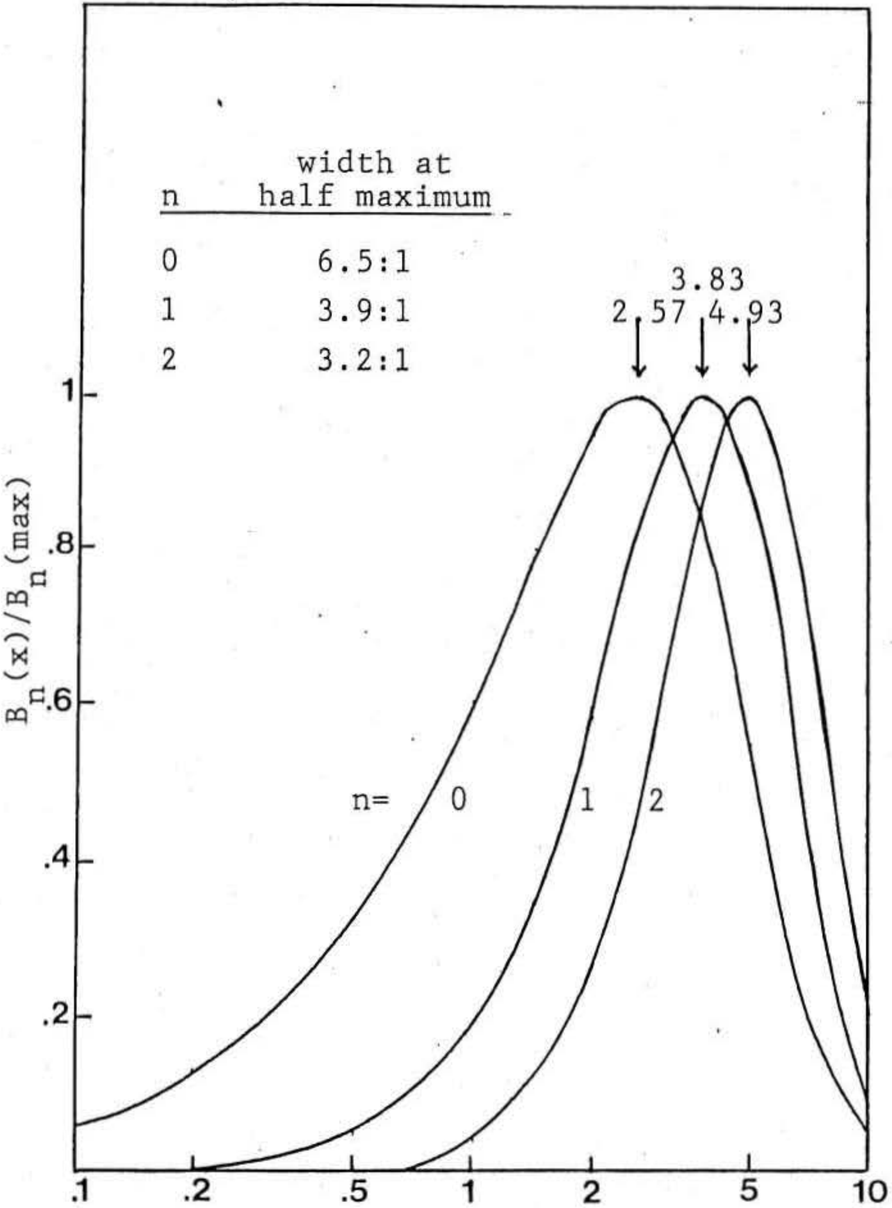

Figure 29: Heat Capacity Inversion Basis Functions

$$C = 9R\frac{T^3}{\theta_d^3}\int_0^{x_d}\frac{x^4e^x}{(e^x-1)^2}dx \tag{44}$$

$$C = 3RT^3g_1\int_0^{x_c}\frac{x^4e^x}{(e^x-1)^2}dx \tag{45}$$

From this comparison, it is clear that if g_1 is set equal to $3/\theta_d^3$, it is the same as approximating the lowest frequency modes in the sample with a Debye model.

For a similar reason, γ can not be assigned accurately using this procedure; the electronic component of the heat capacity is a small contribution to the total over most of the temperature range for which data is available. Thus, both g_1 and γ are assigned values based on the low temperature Debye extrapolation. The rest of the parameters are adjusted to minimize the residuals of equation 43 over the temperature range T_c-50K.

The low frequency cutoff at ω_0, which makes integral computation easier, causes insignificant error in the B_2 function, and certainly does not introduce errors into the model heat capacity greater than the experimental error in the data. The high frequency cutoff at ω_5 (400K) is necessary for normalization, and should not cause any loss of information in the final spectra. In the case of pure niobium, there is no significant phonon state density above about 330K[44], and the Nb-Ti spectrum at high temperature should be similar.

The requirement that $F(\omega)$ be normalized (equation 39) is not explicitly enforced by the least squares fitting procedure, but it is encouraged by padding the data set with an artificial point at high temperature with the lattice heat capacity equal to 3R. In this way, deviations from the normalization condition affect the residual error of the fit, and thus drive the procedure towards normalization.

It must be recognized that, for fundamental reasons, any inversion of heat capacity data will generate only a general picture of the actual phonon density of states. However, the main limitation of this technique is it's low resolution; thus, although detailed structure is lost, the trends and relative frequency weights of the spectrum as a whole should be well represented. Work by Lachal et al.[48] indicates that reliable phonon averages can be determined using this procedure even if the details of the model spectra do not accurately reflect those of the actual system.

Table 5 presents the fitting coefficients for each of the alloys as well as the normalization constant, calculated from equation 39. Ideally, this latter quantity should be equal to 1, but for the 35%, 40% and 70% niobium alloys it is closer to 1.5. This may be a sign that the electronic heat capacity has been underestimated for these alloys, forcing the fitting routine to increase the phonon density of states at higher temperatures to compensate. All but the 70% alloy show a higher density of phonons in the 5 to 10 meV energy range (50-100K) than would be expected from a simple Debye model, with the greatest enhancement in the 35% alloy. The spectrum of the 70% alloy is most enhanced at even lower energies (25-50K). The general trend is for the phonon density of modes at lower energies to be increased beyond that of the Debye spectrum, and that at high energies to be reduced.

% Nb	γ (mJ/mol-K^2)	g_1 (6-25)	g_2 (25-50)	g_3 (50-100)	g_4 (100-200)	g_5 (200-400)	N
20	5.0	1.81	1.79	1.92	1.42	.305	.95
25	5.0	1.99	1.78	2.34	1.46	.332	1.03
30	8.8	2.37	2.19	2.70	1.43	.331	1.03
35	7.5	3.11	2.89	3.63	1.11	.589	1.46
40	8.6	2.68	2.40	3.13	1.44	.379	1.46
50	5.8	2.45	2.26	2.81	1.43	.459	1.26
60	5.2	2.39	2.26	2.63	1.62	.405	1.21
70	4.7	2.25	2.54	2.17	1.41	.570	1.45

all g values multplied by 10^7

Table 5: Lattice Heat Capacity Fit Parameters

14 Predicted and Measured Critical Fields

Using the data and equations presented in the previous sections, it is possible to calculate WHH predictions for each of the Nb-Ti alloys in this study. First, the phonon density of states can be combined with equation 37 to calculate ω_ℓ, the average phonon frequency, for each sample. This calculation is based on the assumption, discussed earlier, that $\alpha^2(\omega)$ is constant. Then, with T_c, ω_ℓ, and an assumed μ^*, the Allen and Dynes equation yields λ_{ep}, the electron-phonon coupling constant. The T_c derived from the H_{c_2} extrapolation to H=0 seems most appropriate for use in this calculation. Finally, equations 29 and 24, together with the resistivity dH_{c_2}/dT, and γ data previously presented determine α_n and α_s. These results are listed in table 6.

The primary problem illustrated by this analysis is that the α values determined by superconducting measurements and normal state measurements do not agree. Such behavior has been noticed in Nb-Ti before[23], although not over such a wide range of compositions. It is possible that this is because the Boltzmann equation, used in the determination of α_n, does not accurately describe the Nb-Ti system. This equation is valid when the fermi surface is spherical and only elastic scattering occurs. Typically, umklapp processes are frozen out at low temperatures, because thermal energy is insufficient to excite phonons with a large enough k vector to cause zone to zone scattering. In the niobium based alloys, however, the soft

$< 111 >$ phonon can be excited with very little energy, and this mode may be able to cause inelastic scattering.

In an attempt to decide which of these two measures of α were more meaningful, each was used to generate a fit to the H_{c_2}(T) data with the WHH equation. These fits are plotted along with H_{c_2} data for each of the alloys in figures 30-37. The spin-orbit scattering parameter, λ_{so}, was varied freely in this process, to minimize the RMS deviation from the data. For the α_s based fits, this worked rather well, and the λ_{so} corresponding to the best fit is also listed in the table. However, the H_{c_2} behavior of only one alloy (70%) could be fit using the α_n values; all other fits showed significant discrepancies. The fits based on α_s generally indicated that spin-orbit scattering was negligible, nearly zero in all cases but the 70% alloy. For the 60% alloy, it was not possible to accurately fit the low temperature data, since even with λ_{so} set equal to zero, the WHH prediction was .6T too high at 2K.

The errors in this fitting procedure result solely from errors in determining α, and these are dominated by the error in μ^* used in the Allen and Dynes equation. As a result of sensitivity analysis of this equation, it appears that for the range of parameters found in the Nb-Ti system ($T_c \approx 9$K, $\omega_\ell \approx 170$K), the variation in λ_{ep} due to μ^* is about 1/3 the percentage error in μ^*. Since the uncertainty in μ^* is about 30-40%, and thus the uncertainty in λ_{ep} is around 10%, then α can only be determined to about 5%. On this level of accuracy, the H_{c_2}data for the samples with 20% to 50% niobium can all be described by assuming that there is

% Nb	ω_ℓ	λ_{ep}	α_n	α_s	λ_{so}
20	166	.85	.42	.74	.3
25	165	.91	.48	.89	.1
30	159	.95	.77	.88	0
35	174	.93	.56	.81	.1
40	160	.98	.56	.76	.05
50	171	.96	.31	.66	.1
60	167	.99	.31	.55	0
70	186	.94	.16	.41	10

Table 6: WHH Fit Parameters

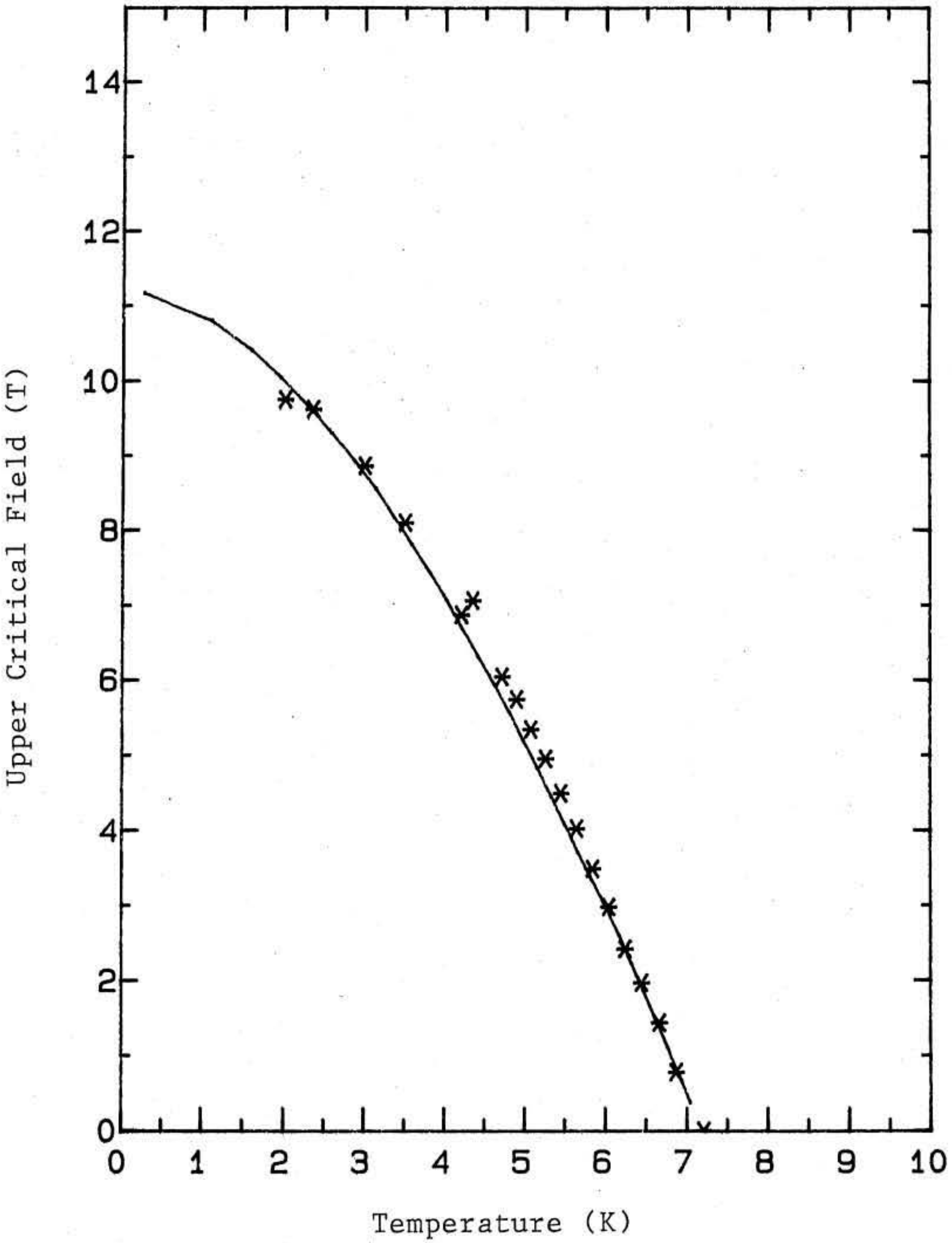

Figure 30: WHH Fit for 20% Niobium Alloy

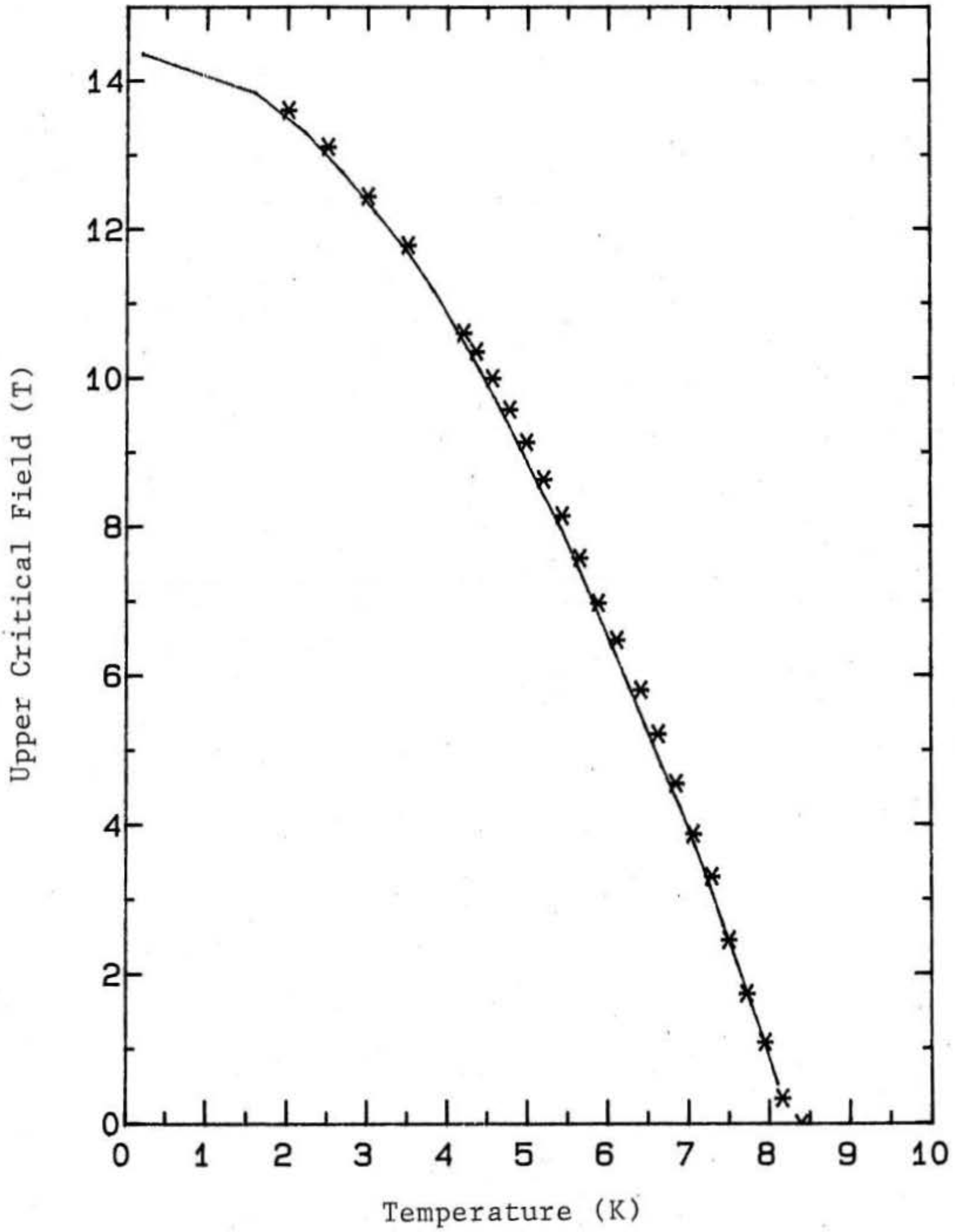

Figure 31: WHH Fit for 25% Niobium Alloy

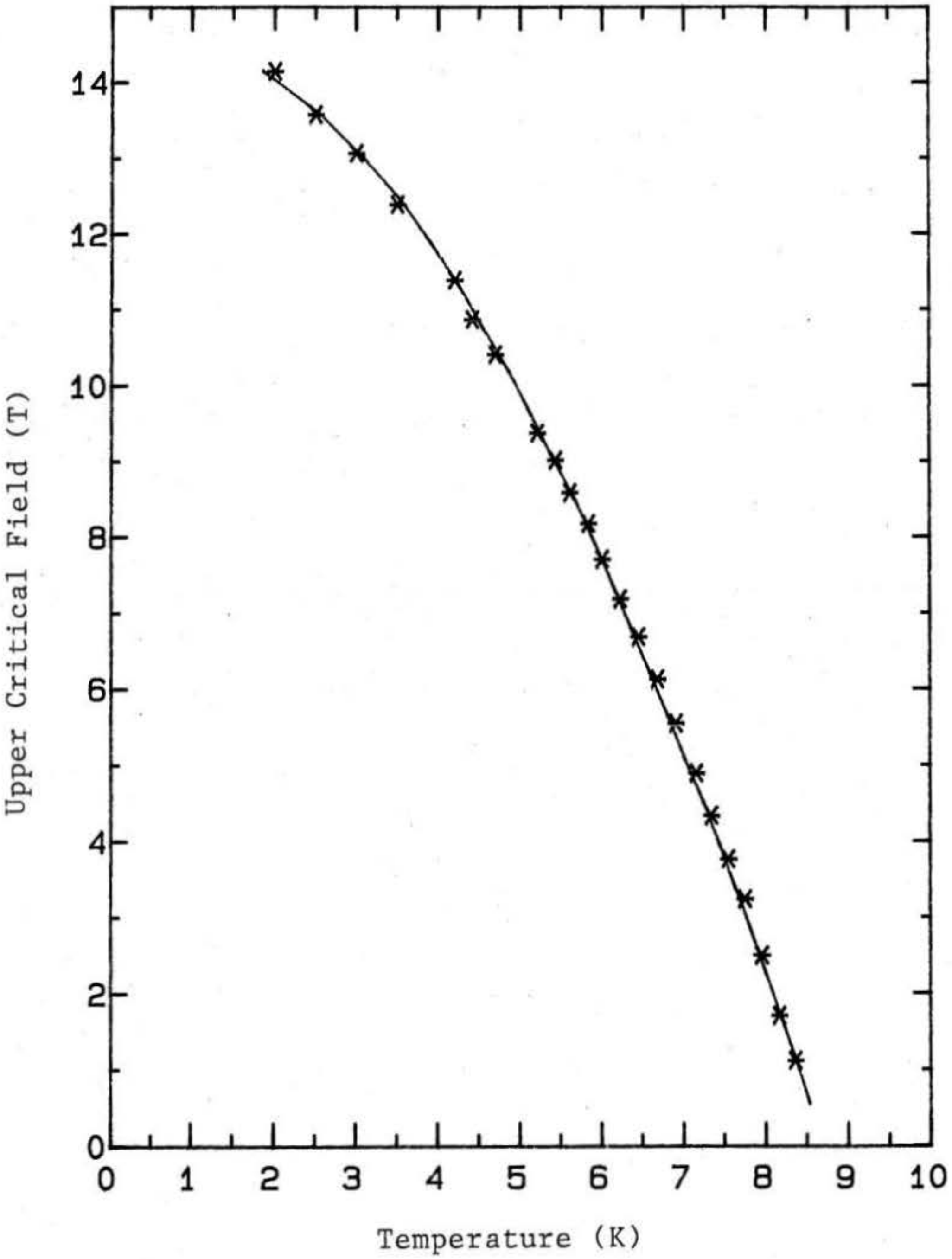

Figure 32: WHH Fit for 30% Niobium Alloy

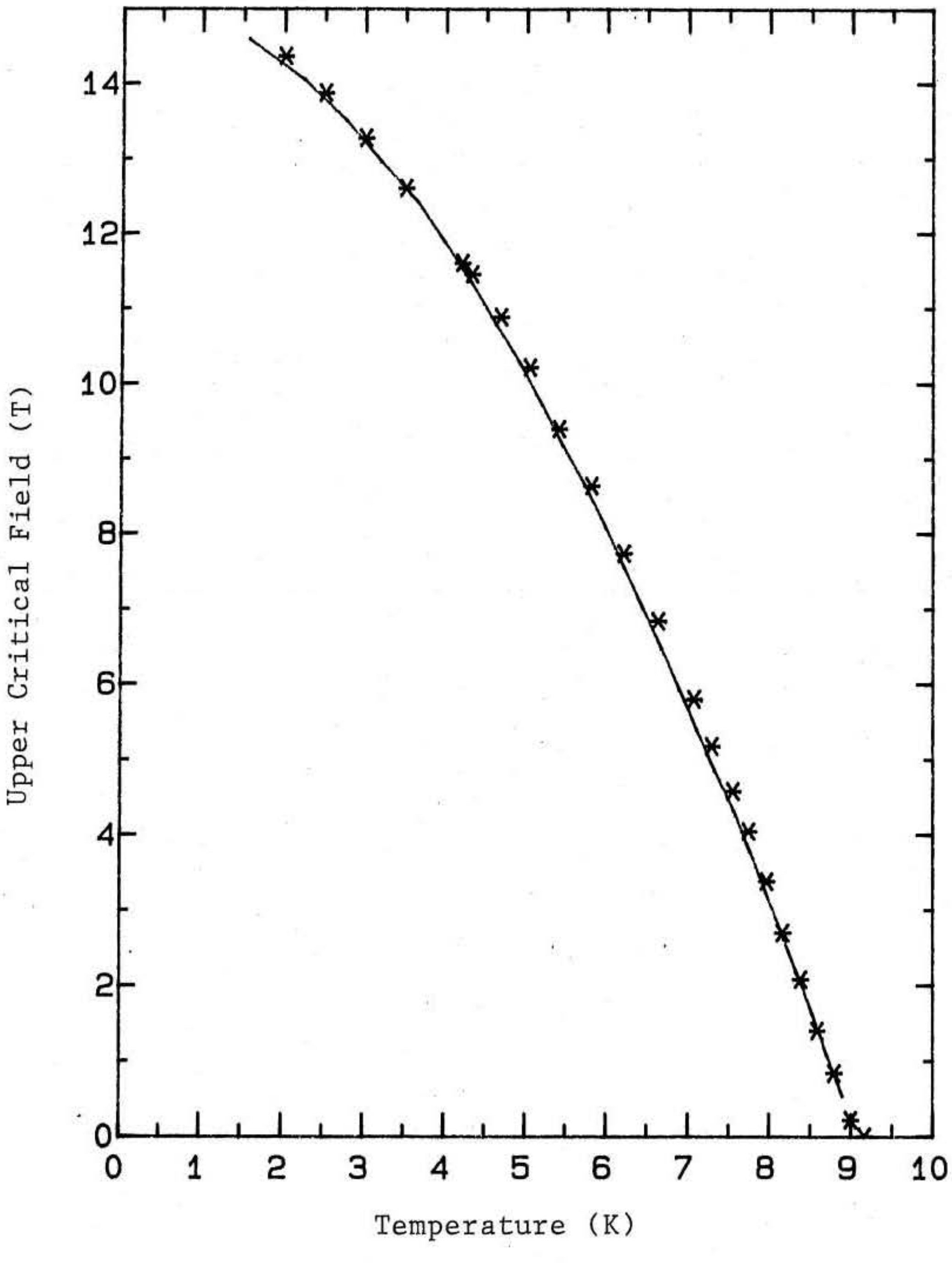

Figure 33: WHH Fit for 35% Niobium Alloy

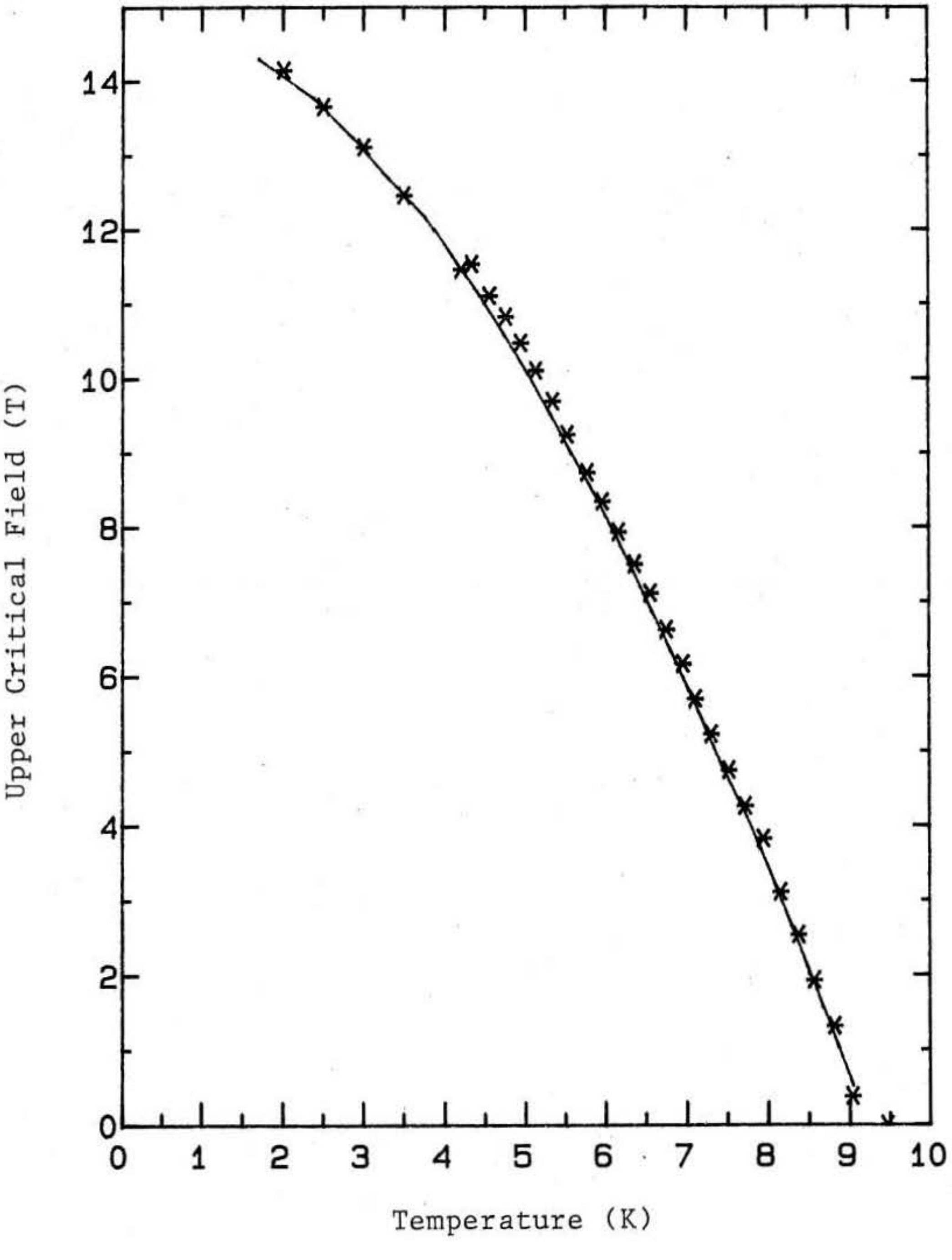

Figure 34: WHH Fit for 40% Niobium Alloy

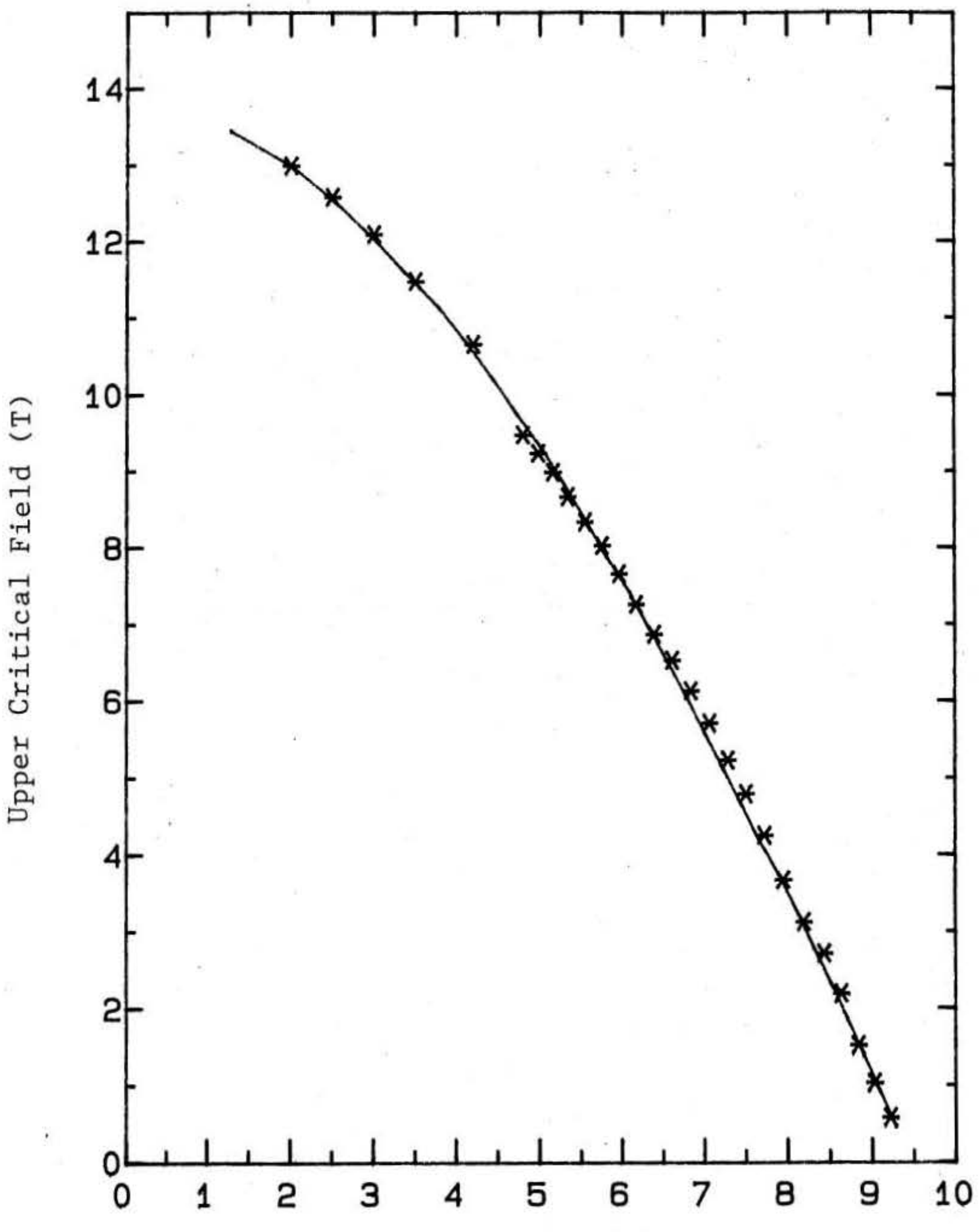

Figure 35: WHH Fit for 50% Niobium Alloy

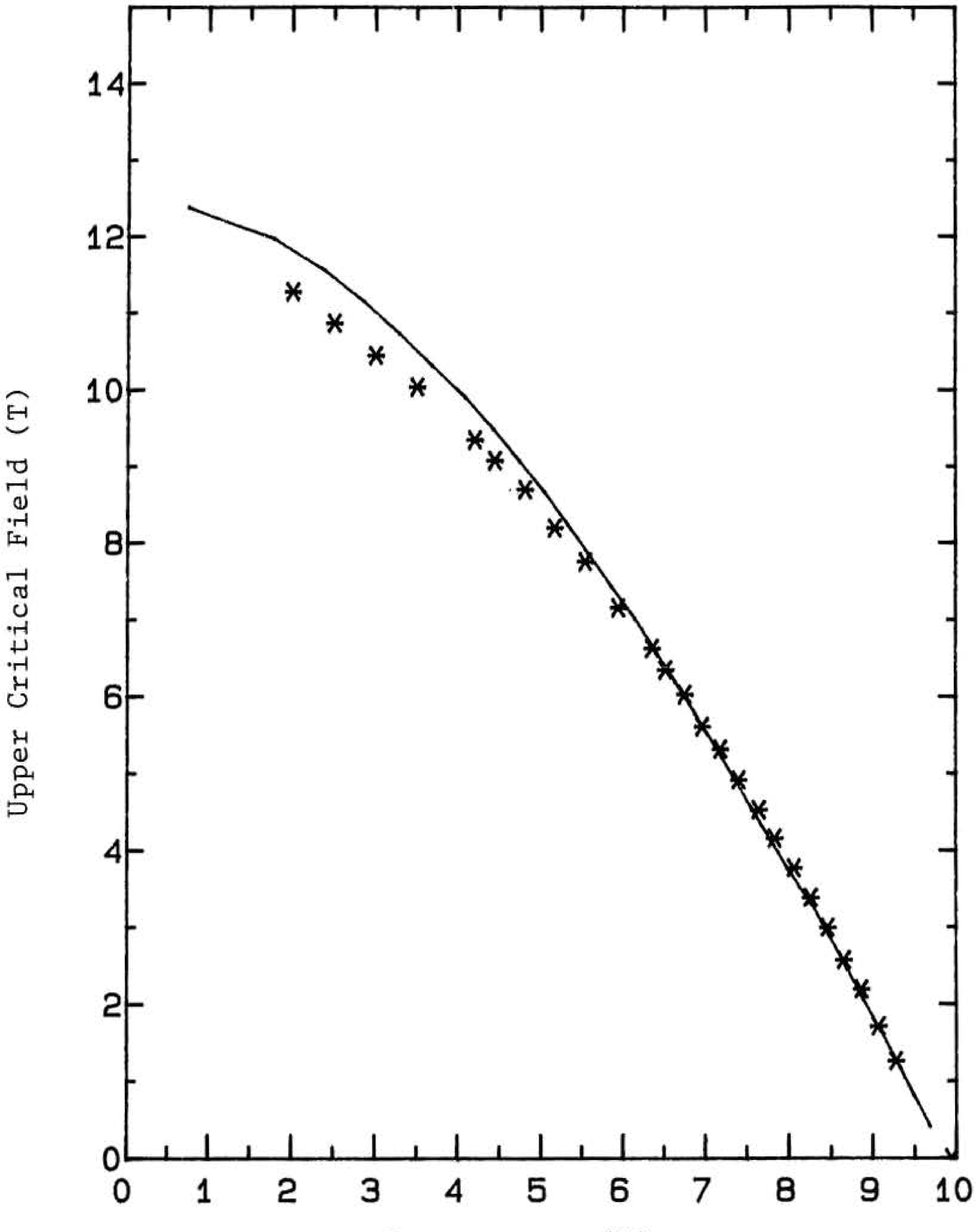

Figure 36: WHH Fit for 60% Niobium Alloy

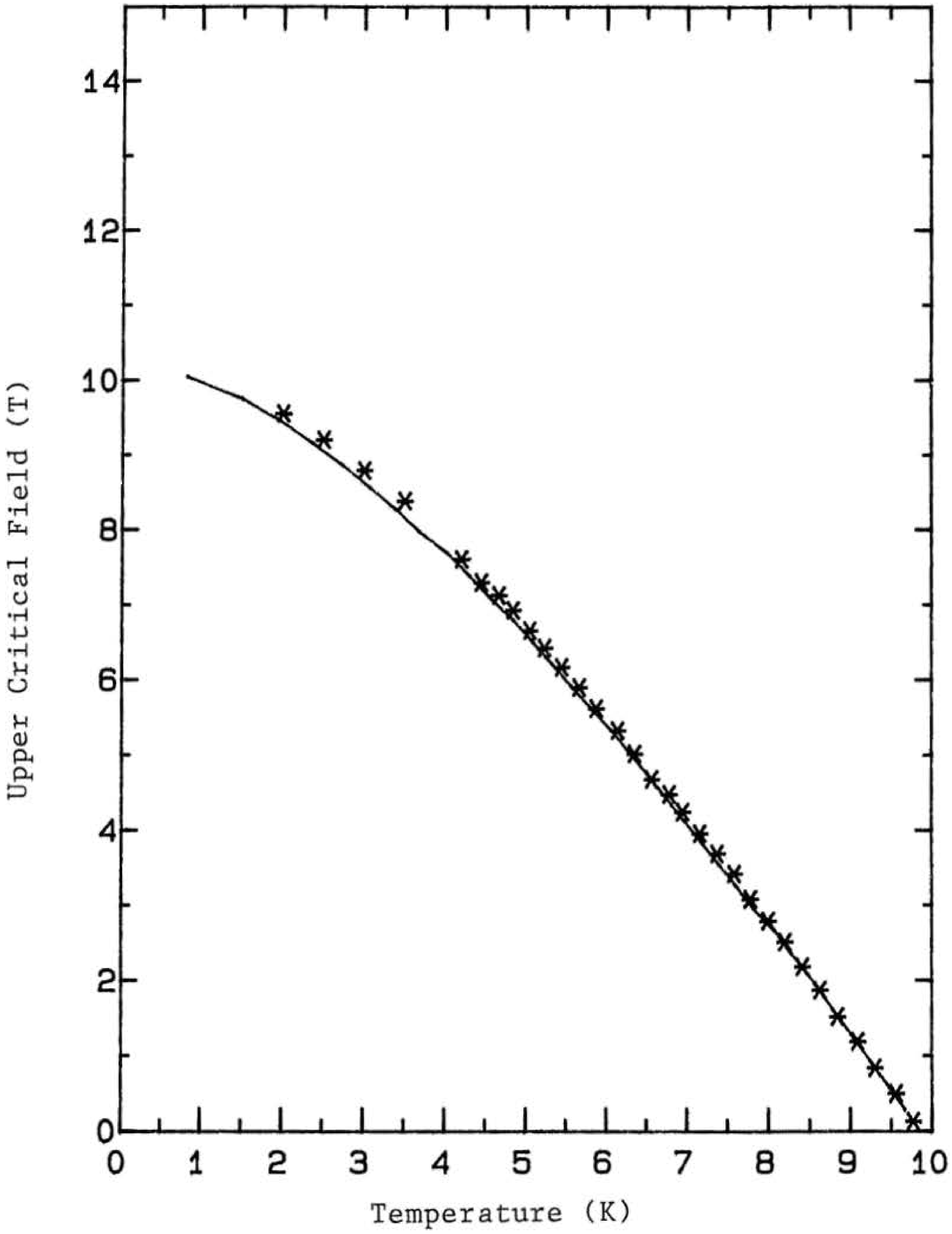

Figure 37: WHH Fit for 70% Niobium Alloy

no spin-orbit scattering. The 60% niobium alloy data cannot be described well at low temperatures, and the 70% niobium alloy can be fit only if appreciable spin-orbit scattering is assumed. There does not seem to be a sensible explanation for this erratic behavior of the high niobium content alloys.

Another interesting point to note is that the alloys in this study, especially the high titanium compositions, are almost localized. One measure of the degree of localization is the product $k_f\ell$, which can be reexpressed as $(mv_f/h)(v_f\tau)$, which in turn is equal to $3/2\alpha$. This value can be as low as 1.5 for the studied alloys, which indicates that they are weakly localized. Localization effects are certainly not included in the WHH treatment, even with renormalization corrections. The effect of this weak localization on $H_{c_2}$is not clear for a bulk material, and is perhaps worth further consideration.

In summary, renormalization corrections to the WHH theory significantly change the description of the H_{c_2} behavior of Nb-Ti. While the alloy is conventionally treated as a paramagnetically limited material, the revised theory indicates that paramagnetic limitation is not of major importance. Thus, enhancements in H_{c_2} that result from ternary additions of tantalum to the Nb-Ti base alloy are unlikely to be due to relaxation of paramagnetic constraint. Such constraint does not actually exist in the binary alloy, but only appears to because renormalizations are ignored. Further, one of the equations embedded in the WHH derivation, relating γ, ρ_n, and dH_{c_2}/dT, is not satisfied for the alloys studied. This equation, known in one form as the Goodman equation, is quite inaccurate over the whole composition range, especially so in the niobium rich alloys. This is perhaps due to the soft phonon mode present in niobium alloys, which could render invalid the Boltzmann equation used in the derivation.

References

[1] N.R. Werthamer, E. Helfand, P.C. Hohenberg, Phys. Rev. 147, p. 295, (1966).

[2] L.J. Neuringer, Y. Shapira, Phys. Rev. Lett. 17, p. 81, (1966).

[3] D.C. Larbalestier, D.G. Hawksworth, *Advances in Cryogenic Engineering (Materials)*, vol. 26, p. 479. ed. A.F. Clark, R.P. Reed, Plenum Press, New York, (1980).

[4] T.P. Orlando, E.J. McNiff, S. Foner, M.R. Beasley, Phys. Rev. B 9, p. 4545, (1979).

[5] A.M. Clogston, Phys. Rev. Lett. 9, p. 266, (1962).

[6] D.L. Moffat, Ph.D. Thesis, University of Wisconsin-Madison (1985).

[7] D.L. Moffat, D.C. Larbalestier, Met. Trans. A 19A, p. 1677, (1988).

[8] M. Hansen, E.L. Kamen, H.D. Kessler, D.J. McPherson, Trans. of TME-AIME 191, p. 881, (1951).

[9] E.W. Collings, *Applied Superconductivity, Metallurgy, and Physics of Titanium Alloys (vol. 1, Fundamentals)*, p. 21. Plenum Press, New York, (1986).

[10] A.R.G. Brown, J.A. Gray, K.S. Jepson, *The Science, Technology, and Applications of Titanium*, p.667. ed. R.I. Jaffee, N.E. Promisel, Pergamon Press (1970).

[11] D. DeFontaine, Acta Met. 18, p. 275, (1970).

[12] N. Wakabayashi, Phys. Rev. B 33, p. 6771, (1986).

[13] R.K. Vohra, S.K. Sikha, R. Chidambaram, Jour. Phys. F 9, p. 1771, (1979).

[14] A.T. Balcerzak, S.L. Sass, Met. Trans. 3, p. 1601, (1972).

[15] D.C. Larbalestier, A.W. West, W. Starch, W. Warnes, P. Lee, W.K. McDonald, P. O'Larey, K. Hemachalam, B. Zeitlin, R. Scanlan, C. Taylor, IEEE Trans. Mag. MAG-21 2, p. 269, (1985).

[16] A.F. Prekul, V.A. Rassokin, N.V. Volkenshtein, Sov. Phys. JETP 40, p. 1134, (1974).

[17] E.W. Collings, Phys. Rev. 9, p. 3989, (1974).

[18] T.G. Berlincourt, A.R. Hake, Phys. Rev. 131, p. 140, (1963).

[19] U. Zweicker, T. Meier, E. Roschel, Z. Metall. 61, p. 836, (1970).

[20] W.N. Lawless, Rev. Sci. Inst. 46, p. 625, (1975).

[21] K.M. Ralls, Ph.D. Thesis, Massachusetts Institute of Technology, (1964).

[22] P.H. Bellin, H.C. Gatos, V. Sadagopan, Jour. App. Phys. 41, p. 2057, (1970).

[23] R.A. Brand, Ph.D. Thesis, Cornell University, (1972).

[24] D.B. Smathers, Ph.D. Thesis, University of Wisconsin-Madison, (1984).

[25] M. Suenaga, K.M. Ralls, Jour. App. Phys. 40, p. 4457, (1969).

[26] J.K. Hulm, R.D. Blaugher, Phys. Rev. 123, p. 1569, (1961).

[27] E.M. Forgan, S. Nedjat, Rev. Sci. Inst. 51, p. 411, (1980).

[28] W.N. Lawless, C.F. Clark, R.W. Arenz, Rev. Sci. Inst. 53, p.1647, (1982).

[29] S. Riegel, G. Weber, Rev. Sci. Inst. 19, p. 790, (1986).

[30] A. Savitsky, M.J.E. Golay, Anal. Chem. 36, p. 1627, (1964).

[31] D.W. Osborne, H.E. Flotow, F. Schreiner, Rev. Sci. Inst. 38, p. 159, (1967).

[32] R.J. Corrucini, J.J. Gniewek, NBS Monograph 21, (1960).

[33] T. Sasaki, Annual Report of the Reasearch Institute for Iron, Steel, and Other Metals, p. 103, (1985).

[34] E.M. Savitskii, V.V. Baron, Y.V. Efimov, M.I. Bychkova, L.F. Myzenkova, *Superconducting Materials*, p. 230 Plenum Press, New York, (1973).

[35] H.L. Leupold, H.A. Bourse, Phys. Rev. 134, p. 1958, (1964).

[36] J.C. Ho, private communication

[37] L.P. Gorkov, Sov. Phys. JETP 36, p. 1364, (1959).

[38] L.P. Gorkov, Sov.Phys. JETP 37, p. 998, (1960).

[39] A.P. Migdal, Sov. Phys. JETP 7, p. 996, (1958).

[40] P.B. Allen, B. Mitrovic, *Solid State Physics 37*, p. 1, (1982).

[41] G. Grimvall, Phys. Script. 14, p. 63, (1976).

[42] P.B. Allen, R.C. Dynes, Phys. Rev. B 12, p. 905, (1975).

[43] W.L McMillan, J.M. Rowell, Phys. Rev. 148, p. 561, (1966).

[44] W.L. McMillan, Phys. Rev. 167, p. 331, (1968).

[45] B. Mitrovic, H.G. Zarate, J.P. Carbotte, Phys Rev. B 29, p. 184, (1984).

[46] T.P. Orlando, M.R. Beasley, Phys. Rev. Lett. 46, p. 1598, (1981).

[47] A. Junod, T. Jarlborg, J. Muller, Phys. Rev. B 27, p. 1568, (1983).

[48] B. Lachal, A. Junod, J. Muller, Jour. Low Temp. Phys. 55, p. 195, (1984).

[49] R.G. Chambers, Proc. of Phys. Soc. 78, p. 941, (1961).